Geoscience Frontiers 8 (2017) 1115–1133

HOSTED BY

Contents lists available at ScienceDirect

China University of Geosciences (Beijing)

Geoscience Frontiers

journal homepage: www.elsevier.com/locate/gsf

Research paper

Distinct metamorphic evolution of alternating silica-saturated and silica-deficient microdomains within garnet in ultrahigh-temperature granulites: An example from Sri Lanka

P.L. Dharmapriya [a,b,c], Sanjeewa P.K. Malaviarachchi [a,b,*], Leo M. Kriegsman [c,d], K. Sajeev [e], Andrea Galli [f], Y. Osanai [g], N.D. Subasinghe [h], C.B. Dissanayake [b]

[a] Postgraduate Institute of Science, University of Peradeniya, 20400, Sri Lanka
[b] Department of Geology, Faculty of Science, University of Peradeniya, 20400, Sri Lanka
[c] Department of Geology, Naturalis Biodiversity Center, Darwinweg 2, 2333 CR, Leiden, The Netherlands
[d] Department of Earth Sciences, University of Utrecht, NL-3584 CD, Utrecht, The Netherlands
[e] Center for Earth Sciences, Indian Institute of Science, Bangalore, 560012, India
[f] Department of Earth Sciences, ETH Zurich, Sonnegstrasse 5, CH-8092, Zurich, Switzerland
[g] Division of Earth Sciences, Department of Environmental Changes, Faculty of Social and Cultural Studies, Kyushu University, 744 Motooka, Fukuoka, 819-0395, Japan
[h] National Institute of Fundamental Studies, Hantana Road, Kandy, Sri Lanka

ARTICLE INFO

Article history:
Received 12 June 2016
Received in revised form
29 October 2016
Accepted 4 November 2016
Available online 8 December 2016
Handling Editor: H.M. Rajesh

Keywords:
UHT
Metapelites
Garnet
Microdomains
Highland Complex
Sri Lanka

ABSTRACT

Here we report the occurrence of garnet porphyroblasts that have overgrown alternating silica-saturated and silica deficient microdomains via different mineral reactions. The samples were collected from ultrahigh-temperature (UHT) metapelites in the Highland Complex, Sri Lanka. In some of the metapelites, garnet crystals have cores formed via a dehydration reaction, which had taken place at silica-saturated microdomains and mantle to rim areas formed via a dehydration reaction at silica-deficient microdomains. In contrast, some other garnets in the same rock cores had formed via a dehydration reaction which occurred at silica-deficient microdomains while mantle to rim areas formed via a dehydration reaction at silica-saturated microdomains. Based on the textural observations, we conclude that the studied garnets have grown across different effective bulk compositional microdomains during the prograde evolution. These microdomains could represent heterogeneous compositional layers (paleobedding/laminations) in the precursor sediments or differentiated crenulation cleavages that existed during prograde metamorphism. UHT metamorphism associated with strong ductile deformation, metamorphic differentiation and crystallization of locally produced melt may have obliterated the evidence for such microdomains in the matrix. The lack of significant compositional zoning in garnet probably due to self-diffusion during UHT metamorphism had left mineral inclusions as the sole evidence for earlier microdomains with contrasting chemistry.

1. Introduction

Garnet is a common mineral formed in a wide range of pressure-temperature conditions from lower greenschist facies rocks to ultrahigh-temperature (UHT) granulites and ultrahigh-pressure (UHP) eclogites. Microstructural relationships, e.g., inclusion phases and patterns, and chemical and isotopic zoning in garnet provide useful records of metamorphic processes and rates (Ague et al., 2012; Ague and Carlson, 2013; Caddick and Kohn, 2013), especially in medium-grade metamorphism. In most high-grade granulite terrains, however, the prograde evidence is frequently obliterated due to strong ductile deformation-associated high to ultrahigh temperatures.

In the literature, garnet growth is commonly attributed to a single metamorphic reaction or to a series of successive reactions

* Corresponding author. Department of Geology, Faculty of Science, University of Peradeniya, 20400, Sri Lanka.
E-mail address: malavi@pdn.ac.lk (S.P.K. Malaviarachchi).
Peer-review under responsibility of China University of Geosciences (Beijing).

http://dx.doi.org/10.1016/j.gsf.2016.11.008

assuming constant bulk chemistry for the reaction domain. Complications that have been taken into account include melt loss that changes the chemistry of the reaction domain in a homogeneous manner (e.g., White et al., 2003). However, medium-grade garnet has commonly been observed to overgrow micro-layers with highly contrasting chemistries either reflecting original layering or differentiated crenulation cleavages. Classical examples are snowball garnets discussed by structural geologists (e.g., Schoneveld, 1977; Bell and Cuff, 1989; Kim and Bell, 2005). As a result, garnet grains with dimensions larger than the diffusion path lengths of major elements in the microtextures may be expected to show subdomains that have formed by different metamorphic reactions.

We report here the growth of large, single garnet grains in UHT metapelitic granulites from the Highland Complex, Sri Lanka, via different mineral reactions in silica-saturated and silica-deficient bulk compositions. In this context, we propose a model to explain the formation of such complex garnets and show that such garnet bearing mineral assemblages require multiple pseudosections to reconstruct their *P-T* history.

2. Geological setting and sample description

2.1. Geological setting

Sri Lanka is a small but important crustal fragment in the East Gondwana. Based on Nd model age determinations (Milisenda et al., 1988, 1994) and lithological characteristics, the basement rocks of Sri Lanka have been subdivided into four lithotectonic units (e.g., Kröner et al., 1991; Cooray, 1994) named as the Wanni Complex (WC), Kadugannawa Complex (KC), Highland Complex (HC) and Vijayan Complex (VC; Fig. 1a). All samples related to this study were collected near the WC-HC boundary (Fig. 1a and b).

The HC yields Nd model ages of 3400–2000 Ma (Milisenda et al., 1988, 1994; Höl1zl et al., 1991, 1994; Kröner et al., 1994a; Malaviarachchi and Takasu, 2011a), evolved during the assembly of Gondwana Super Continent. The HC is composed of granulitic metaquartzites, metapelitic gneisses, marbles, calc-silicate granulites and charnockites (e.g., Cooray, 1994; Mathavan and Fernando, 2001). The detrital zircon ages are in the range of ca. 3200–1900 Ma and hence the deposition of sediments of the HC had taken place prior to ca. 1900 Ma. Most of the granitoid plutons later transformed into orthogneisses, subsequently intruded into the sediments at 1900–1800 Ma and 670 Ma (Höl1zl et al., 1994; Kröner et al., 1994a; Santosh et al., 2014). High to ultra-high temperature metamorphic ages of the rocks of the HC varies in the range of 610–530 Ma (Höl1zl et al., 1991, 1994; Kröner et al., 1994a; Malaviarachchi and Takasu, 2011a; Santosh et al., 2014; Dharmapriya et al., 2015b; Takamura et al., 2016). Syntectonic and post-tectonic pulses of mafic and charnockitic magmatism have also been reported in the HC (e.g., Santosh et al., 2014). Further, recent studies reported incorporation of Neoproterozoic detrital zircons in the HC metasediments (Dharmapriya et al., 2015b, 2016; Osanai et al., 2016b; Takamura et al., 2016).

In the HC, metamorphic pressures and temperatures (*P-T*) decrease from 8–9 kbar and 800–900 °C in the east and southeast to 4.5–6 kbar and 700–750 °C in the southwest (Faulhaber and Raith, 1991; Kriegsman, 1994, 1996; Raase and Schenk, 1994; Schumacher and Faulhaber, 1994; Kriegsman and Schumacher, 1999; Malaviarachchi and Takasu, 2011b; Dharmapriya et al., 2014a). UHT granulites have been reported only from few localities in the central HC (Osanai, 1989; Kriegsman and Schumacher, 1999; Bolder-Schrijver et al., 2000; Osanai et al., 2000, 2006, 2016a,b; Braun and Kriegsman, 2003; Sajeev and Osanai, 2004a; Sajeev et al., 2007, 2010; Dharmapriya et al., 2015a,b, 2016; Malaviarachchi and Dharmapriya, 2015) and rarely in the southwestern part (Sajeev and Osanai, 2004b) from pelitic, mafic and quartzofeldspathic granulites. Estimated *P-T* conditions of UHT granulites are in the range of 900–1150 °C at *P* of 9–12.5 kbar (Kriegsman and Schumacher, 1999; Sajeev and Osanai, 2004a,b; Osanai et al., 2006; Sajeev et al., 2007, 2010; Dharmapriya et al., 2015a,b, 2016).

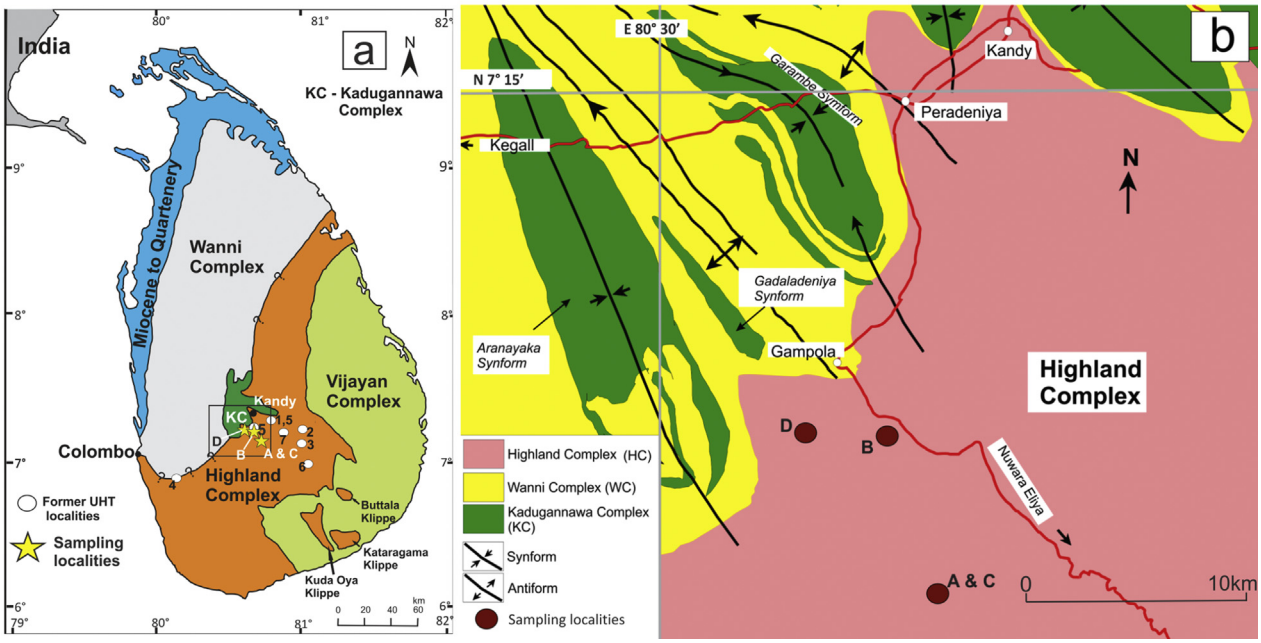

Figure 1. (a) Geological map of Sri Lanka showing the lithotectonic subdivision (after Cooray, 1994). A star shows sampling locality and circles show UHT localities reported so far: 1. Osanai (1989): $T = 900$ °C; 2 & 3. Kriegsman and Schumacher (1999): $T = 830$ °C (here it is corrected as 950 °C); 4. Sajeev and Osanai (2004a): $T = 950$ °C; 5. Sajeev and Osanai (2004b): $T = 1150$ °C; 6. Osanai et al. (2006): $T = 1000$ °C; 7. Sajeev et al. (2007): $T = 925$ °C; 8. Dharmapriya et al. (2015a): 950–975 °C. (b) Detailed geological map (modified after Kröner et al., 2003) and the sampling localities.

The WC, KC and VC have yielded Nd model ages 2000–1000 Ma, 1600–1000 Ma and 1800–1000 Ma (Milisenda et al., 1988, 1994) respectively and metamorphosed under granulite to amphibolite facies conditions (e.g., Kröner et al., 1991, 2013; Cooray, 1993, 1994, 1996; Mathavan et al., 1999). The reader is referred to Santosh et al. (2014), Dharmapriya et al. (2016) and He et al. (2016a,b) for further details.

2.2. Sample description

Sapphirine, spinel, gedrite and sillimanite bearing garnet-orthopyroxene gneiss (Rock A) was collected from a quarry at Kotmale (Supplementary file 1a). Rock A occurs as thin layers (about 20–30 cm in size) in the upper portion of the quarry of which the main lithology is garnet-orthopyroxene ± clinopyroxene gneiss (metadioritic to charnockitic). The sample contains garnet-rich layers (thickness ~2 cm) parallel to the major foliation (Supplementary file 1b,c), demarcated by stretched quartz grains. Garnet in these layers are rimmed by tiny biotite flakes (<0.2–0.4 mm).

Sapphirine, kyanite and spinel bearing garnet-sillimanite-orthopyroxene gneiss (Rock B) was collected from a quarry from Gampola (Supplementary file 1d) south of Kandy. This foliated rock is composed of well-defined compositional domains with gradual variation from one domain to the other without a sharp contact, probably indicating variations of bulk composition within the same rock (Dharmapriya et al., 2015b). The Rock B (Supplementary file 1e) comprises porphyroblastic garnet (0.5–2.5 cm in diameter) surrounded by symplectites of orthopyroxene-cordierite and/or coronas of orthopyroxene-sillimanite (Supplementary file 1e). Leucosomes with subhedral to anhedral quartz and feldspar and tiny flakes of biotites may have formed during the retrograde evolution.

Sapphirine and spinel bearing garnet-sillimanite gneiss (Rock C) occurs as relatively large fragments (25–50 cm size) within the upper portion of the same quarry (Supplementary file 1a) in which the Rock B was collected. The samples contain garnets in various sizes (<0.25 to >3 cm in diameter, Supplementary file 1f,g), locally rimmed by symplectites of orthopyroxene + cordierite (Supplementary file 1g). Ribbon quartz (up to 6 cm in diameter) defines the main foliation. Medium- to fine-grained sillimanite needles are also present within ribbon quartz and show the same orientation. Local clusters of tiny biotite flakes have probably formed during a retrograde stage (Supplementary file 1f).

Corundum, kyanite and staurolite bearing garnet-sillimanite-graphite gneiss (Rock D, typical khondalite) was collected from a road exposure further south of Gampola (Supplementary file 1h) and, contains various sizes of porphyroblastic garnet (0.25–3 cm in diameter, Supplementary file 1i), locally showing euhedral crystal shapes.

3. Petrography and textural evolution of garnet porphyroblasts

We have subdivided the porphyroblastic garnet grains into (1) core, being the most central part of the grain; (2) rim, i.e. the outermost part of the garnet grain, generally a few 100 μm thick; and (3) mantle, being the area between (1) and (2). The absolute size of each domain is variable and depends on the garnet grain size. Mineral Abbreviations are after Kretz (1983).

3.1. Rock A

Rock A contains medium-grained subhedral to anhedral garnet porphyroblasts, (diameter about 0.5–1 cm). The distribution of inclusion phases in garnet is heterogeneous. Sapphirine, spinel, gedrite and sillimanite inclusions occur only within garnet grains that are concentrated in garnet rich layers (Grt_1). Some of the garnets in the garnet rich layer (Fig. 2a contains rounded and prismatic sapphirine (25–80 μm), anhedral spinel (20–60 μm), tiny, both needle shaped and anhedral sillimanite (<20–150 μm) and gedrite (20–100 μm) and tiny rutile and apatite inclusions toward the core area (Fig. 2b–f). Tiny sapphirine grains are present as isolated inclusions (Fig. 2c,e–g), coexisting with spinel (Fig. 2f). Spinel also forms isolated inclusions (Fig. 2f), coexisting with sapphirine (Fig. 2f) or sillimanite (Fig. 2g). Sapphirine, sillimanite and spinel are always present very close to each other whereas gedrite inclusions are present rarely close to the clusters of sapphirine, spinel and sillimanite (Fig. 2g).

In addition, considerable amount of apatite and rutile (Fig. 2e) together with minor amount of monazite and zircon grains are present at the garnet cores. Fine-grained quartz is present mostly in mantle to rim of the garnet (Fig. 2b–d). Isolated and medium-grained biotites, quartz and sillimanite are also commonly distributed in the mantle (Fig. 2b–d), where biotite and sillimanite shows a folded foliation (Fig. 2b,d). The rim of the garnet is surrounded by biotite (Fig. 2h).

The core area of other garnets of the rock (Fig. 2i) contains gedrite in addition to sapphirine, spinel and sillimanite while quartz and biotite are present in the mantle area (Fig. 2i–k). Gedrite coexists with spinel or sapphirine (Fig. 2l) while some spinel grains occur as isolated inclusions (Fig. 2j and k). Rare sillimanite is also present close to isolated spinel (Fig. 2k). In the mantle area, biotite and quartz are present as isolated grains (Fig. 2i and j).

The inclusion phases within the core areas of the above porphyroblastic garnets could indicate the FMASH ($FeO–MgO–Al_2O_3–SiO_2–H_2O$) reaction:

$$Spl + Ged + Sil => Grt + Spr + V \quad (1)$$

while, the mantle to rim areas of the same garnets testify to further growth of garnet via the reaction:

$$Bt + Sil + Qtz => Grt + Kfs + V/Melt \quad (2)$$

In contrast, a sapphirine, spinel and sillimanite bearing cluster is found towards the rim of one side in some other garnets (Fig. 2m) in garnet-rich layer (Fig. 2n). Biotite is present in both core and rim of the garnet grain (Fig. 2m,o). Although isolated quartz is also present in the mantle and towards the rim (Fig. 2o) in the same garnet, there is no quartz inclusions present in the vicinity of sapphirine, spinel and sillimanite bearing cluster. Inclusion phases of this porphyroblastic garnet indicates that the core formed via reaction (2) and the rim via reaction (1).

Garnet grains, which are further away from the garnet-rich layer, are mostly inclusion-free and contain plagioclase, quartz and biotite as minor inclusion phases (Supplementary file 2a).

The matrix contains, ribbon quartz (up to 5 cm), anhedral to subhedral orthopyroxene (0.5–1.5 cm), subhedral to euhedral plagioclase (<0.25–0.5 cm) and anhedral K-feldspar (<0.1–0.5 cm) as major mineral phases (Supplementary file 2b). The stretched quartz grains demarcate the major foliation. Ilmenite and acicular fine biotite flakes (~0.5 cm in length) are present as minor mineral while monazite and zircon occur as accessory phases. Biotite occurs mainly as an overprinting product of garnet and orthopyroxene.

3.2. Rock B

Rock B contains needle shaped sillimanite, anhedral quartz, plagioclase, K-feldspar, biotite and as major constituent minerals

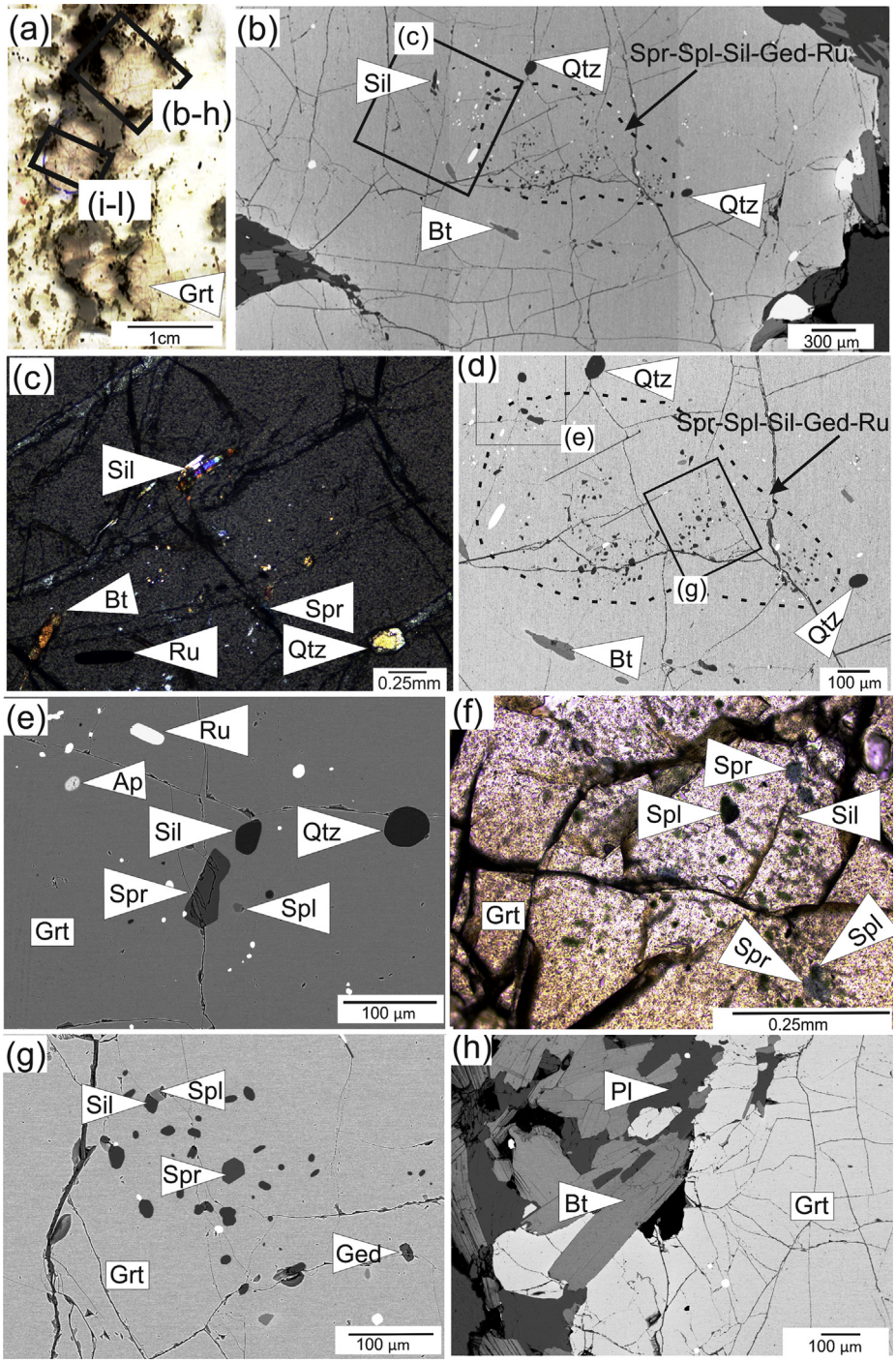

Figure 2. Microtextures of Grt_1 in Rock A (b–h: microtextures of the first Grt_1 grain shown in image (a) in garnet rich layer; i–l: microtextures of the second Grt_1 grain shown in the garnet rich layer; m–o: microtextures of the third Grt_1 grain sown in image (n) in the garnet rich layer). (a) A petrographic thin section representing the garnet rich layer; (b) a mosaic of BSE images of a Grt_1 in which the quartz-deficient core domain and quartz saturated mantle to rim domains are shown; (c) CPL image showing the inclusion phases at the boundary of silica-saturated and silica-deficient domains; (d) closer view of the core area of the garnet in image (c); (e) inclusions of sapphirine, spinel, silimanite and quartz; (f) tiny inclusion phases of garnet coexisting with sapphirne + spinel; (g) coexistence of spinel and sillimanite. Gedrite is also present, (h) formation of biotite + plagioclase corona around garnet; (i) a mosaic of rim of one side to rim of opposite side (cross the core) of a garnet; (j) the image representing the inclusion phases close to the boundary of silica-saturated and silica-deficient domains; (k) BSE image of core area of the garnet, spinel. Tiny sillimanite are also present, (l) closer view of the center part of the image (k) where coexistence of gedrite + sapphirine and gedrite + spinel are present; (m) presence of clusters of spinel-sapphirine-sillimanite toward the rim area of garnet; (n) a thin section representing the garnet of image (o) a mosaic of the garnet in which the rim area of one side contains a silica-deficient domain and the rest of the portion representing a silica saturated domain.

with Fe-Ti oxides (exsolved hematite-ilmenite ± rutile) as a minor phases with sapphirine, kyanite, monazite and zircon as accessory (Fig. 3a–d). Subhedral to anhedral shaped garnets (Grt_2, diameter 0.40–1.5 cm) contains coexisting kyanite + sapphirine at the core area (Fig. 3a–c). Supplementary file 3a shows the Raman spectrum of kyanite. Medium grained kyanite shows approximately prismatic shape (Fig. 3a and b). Isolated quartz is present in the mantle (Fig. 3a and b) area and isolated sillimanite occurs towards the rim area of the same garnet grain (Fig. 3a,d). Biotite is present from mantle to rim (Fig. 3a and b). The coexisting sapphirine + kyanite in

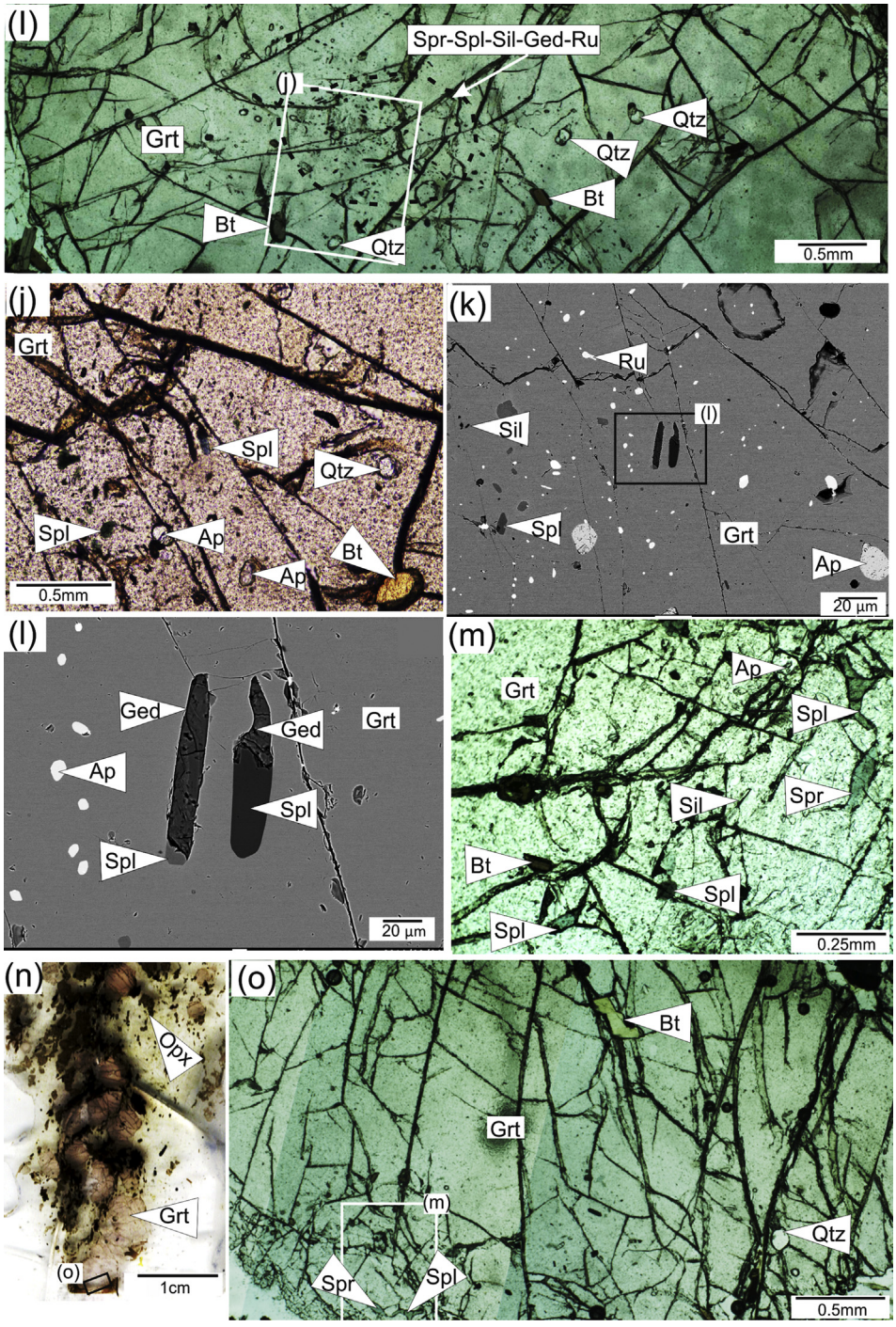

Figure 2. (*continued*)

the core area could have formed via the prograde dehydration reaction in the FMASH system:

$$\text{Mg-rich St} \Rightarrow \text{Spr} + \text{Ky} + \text{Grt} + \text{V} \quad (3)$$

while the isolated sillimanite needles and biotite flakes toward the rim area and presence of quartz towards the outer core area could indicate that a significant portion of Grt_2 has grown via reaction (2).

Staurolite is a common mineral in metasedimentary rocks subjected to Barrovian-type metamorphism (Yardley, 1977), but is also observed in Buchan-type metamorphism, e.g., in the Hercynian domains of the central Pyrenees (Kriegsman, 1989). The reason for the absence of staurolite in Rock B could be the complete

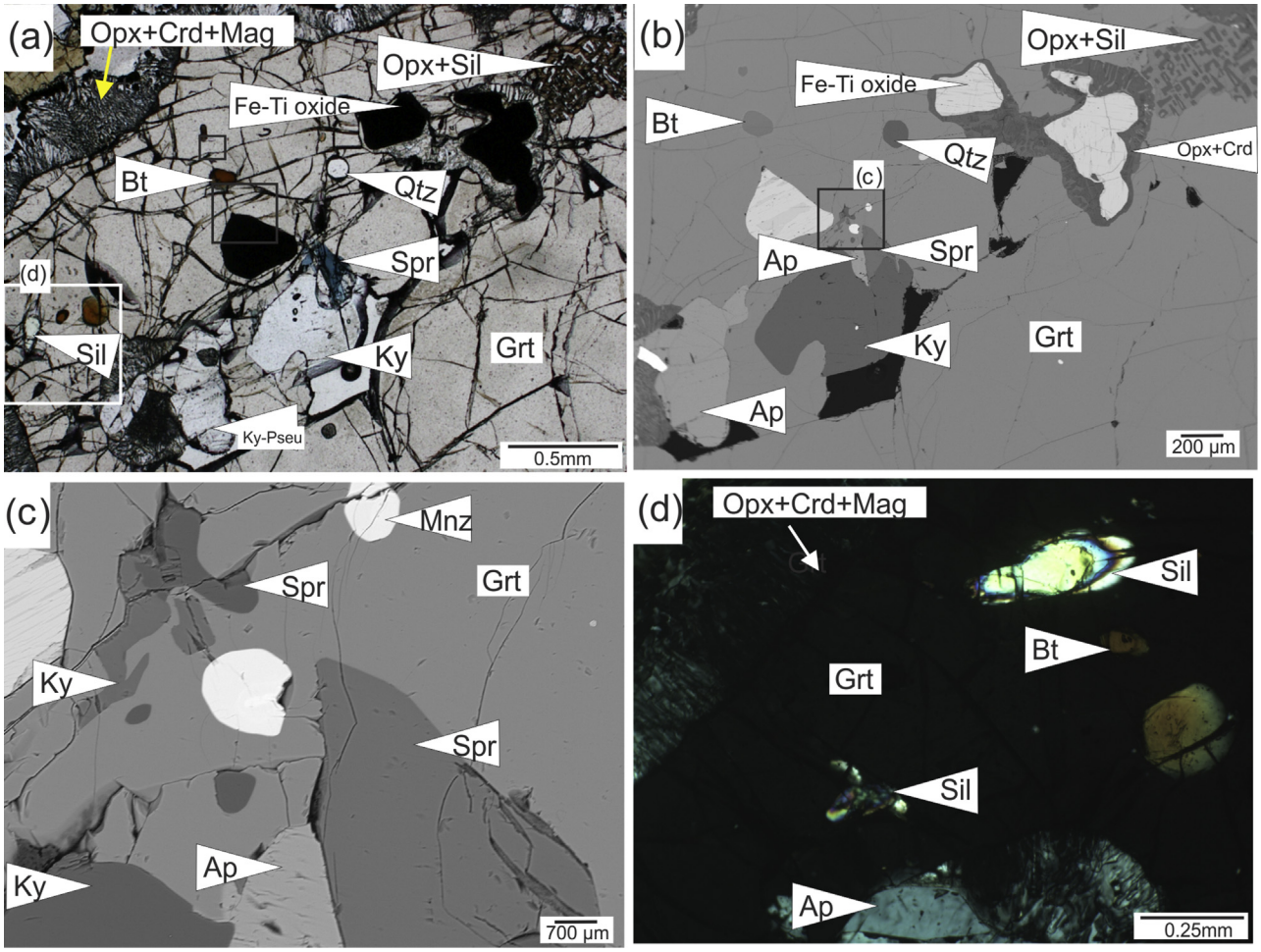

Figure 3. Microtextures of Grt_2 in Rock B. (a) Mineral inclusions from core to rim; (b) BSE image of the image (a); (c) BSE image representing mineral inclusions in the core area; (d) tiny isolated sillimanite inclusion at the rim area.

consumption of staurolite during prograde metamorphism. Theses authors have identified Mg-rich staurolite (X_{Mg} ~0.50) in a locality approximately 2 km west of the sampling locality of Rock B and close to the Victoria dam at the UHT locality 7 in Fig. 1a), in metapelitic granulites. Hiroi et al. (1994) have also reported coexisting local sapphirine + kyanite enclosed by garnet in Highland Complex paragranulites. The authors have also interpreted this assemblage by the operation of reaction (3). Tsunogae and van Reenen (2006) reported on Mg-rich staurolite (X_{Mg} = 0.47–0.52) from the Beitbridge area in the Central Zone, Limpopo Belt of South Africa. The authors regarded the magnesium staurolite as a relict phase and inferred that dehydration reaction (3) took place during prograde metamorphism. Tsunogae and van Reenen (2011) also reported similar examples from the Limpopo Belt.

Most of the garnet grains in the rock are rimmed by orthopyroxene + sillimanite corona (Supplementary file 2c) and/or orthopyroxene + cordierite symplectites (Fig. 3a, Supplementary file 2c,d). At the rim area of some garnet contains a box structure of orthopyroxene-sillimanite (Fig. 3a).

The matrix of the rock B is composed of ribbon quartz (up to 3 cm in length), sillimanite (up to 4 cm in length), subhedral to anhedral K-feldspar (<0.2–0.5 cm) and plagioclase (0.2–0.75 cm) as major mineral phases. Anhedral Fe-Ti oxide (mainly exsolved titanohematite-ilmenite ± rutile grains, Supplementary file 2e) and disseminated biotite flakes (up to 0.25 cm) present as minor constituents while zircon and monazite occur as accessory phases. Fine to medium grained anhedral sapphirine (~200 μm), which are surrounded by two feldspars in some micro domains may represent melt ribs (Supplementary file 2f).

3.3. Rock C

This rock contains subhedral to anhedral, medium to coarse-grained garnet porphyroblasts (Grt_3, diameter about 0.5–2 cm). The garnet grains contain sillimanite, biotite, quartz and rutile as major inclusion phases while plagioclase, K-feldspar and ilmenite as minor phases. Sapphirine, spinel, apatite and zircon are present as accessory phases.

Grains of Grt_3 contain quartz, sillimanite, K-feldspar, biotite, and rutile with minor apatite inclusion phases from core to rim (Fig. 4a and b). In the same grain, clusters of inclusion phases are present at the mantle area in two opposite sides (Fig. 4a–d). These clusters mainly contain sillimanite and rutile as tiny inclusions with no quartz. In some clusters (Fig. 4c and d), tiny sapphirine (~20 μm in length) coexist with sillimanite (Fig. 4e). Close to those inclusions, tiny spinel (~10 μm) and sillimanite co-exist (Fig. 4f). Isolated quartz grains are present surrounding the mineral cluster where the sapphirine and spinel are present (Fig. 4c and d).

Quartz, biotite and sillimanite inclusions from core to rim area indicate that the Grt_3 has mainly grown via reaction (2) in a silica-saturated environment. However, the mantle area of one side of this garnet lacks quartz inclusions and contains the assemblages

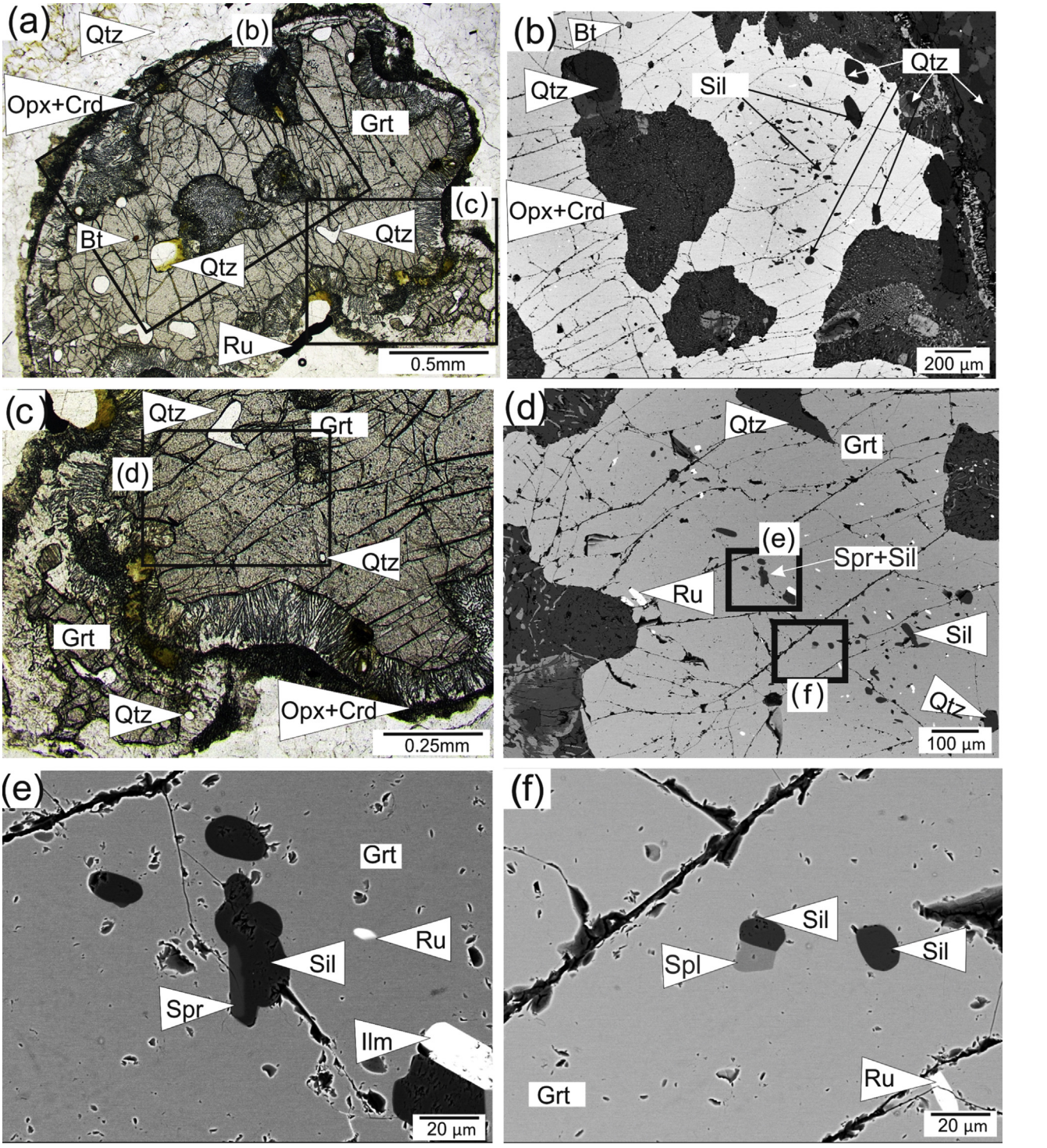

Figure 4. Microtextures of Grt_3 in Rock C. (a) The whole view of the studied garnet; (b) BSE image showing the inclusion phases of core to rim area; (c) the sapphirine and spinel inclusion bearing domain; (d) BSE image showing the sapphirine and spinel bearing domain; (e) BSE image showing coexistence of sapphirine + sillimanite; (f) BSE image showing coexistence of spinel + sillimanite.

sillimanite + spinel and spinel + sapphirine. Hence, this particular garnet domain has grown in a quartz-deficient environment, either by reaction (1) or by an alternative reaction,

$$\text{Mg rich Bt} + \text{Sil} \Rightarrow \text{Grt} + \text{Spl} \pm \text{Spr} + \text{V/Melt} \quad (4)$$

Orthopyroxene-cordierite symplectite is present at the rim of the garnet (Fig. 4a and b). However, some of the Grt_3 lack symplectitic textures (Supplementary file 1g). Sillimanite inclusions in some of these garnets show crenulation lineation (Supplementary file 2g) which is oblique to the major lineation present in the matrix.

In the matrix, garnet, ribbon quartz (up to 5 cm in length), needle shaped sillimanite (from 0.5 to cm in length), fine to medium grained (<0.2–0.5 cm) plagioclase and K-feldspar which is present as recrystallized mineral phases occur as major mineral

phases (Supplementary file 2h). Rutile needles (up to 1 cm in length), tiny biotite flakes (up to 0.4 cm) and ilmenite are present as minor phases while zircon, apatite and monazite represent accessories. Needle shaped sillimanite demarcate the major lineation in the matrix (Supplementary file 2h).

3.4. Rock D

The khondalite contains various sizes of garnet (~0.25–3 cm in diameter). Dharmapriya et al. (2014b) provided detailed description of the microtextures of this rock. Based on inclusion phases four garnet types can be distinguished. The first type of garnet (Type 1) contains sillimanite inclusions at core and kyanite inclusions at rim with staurolite at mantle (Supplementary file 2i,k). The core area of these garnets contains preferredly oriented quartz grains (Supplementary file 2j). The second type of garnet (Type 2) contains corundum, kyanite, spinel sillimanite, quartz and Fe-Ti oxides as inclusions. The third type of garnet (Type 3) has sillimanite, curved quartz and biotite inclusions (Supplementary file 2l) while the fourth type (Type 4) is fine grained garnet with inclusions of sillimanite, rutile and ilmenite (Supplementary file 2m).

Further, it was observed that rarely, the Type 1, Type 3 and Type 4 garnets could be identified in approximately 10 cm × 10 cm sized rock specimens while Type 2 was relatively less abundant and found only in some domains in the matrix where quartz was relatively less abundant compared to the rest of the rock. In this study we used Type 2 garnet (hereafter referred as Grt_4) from this rock.

Grt_4 grains are coarse porphyroblastic (up to 3 cm in diameter), euhedral to subhedral in shape (Fig. 5a). The core and mantle of most of these Grt_4 (Fig. 5a) contain numerous isolated inclusions of anhedral, medium- to fine-grained corundum (0.5–4 mm), which frequently coexist with clusters of fibrolitic sillimanite (Fig. 5b and c). The sillimanite in theses clusters has probably grown as a pseudomorph after kyanite (Fig. 5b and c). Sometimes, Grt_4 contains relatively large (up to 0.5 cm) prismatic sillimanite, which contains plenty of tiny spinel inclusions and rare, tiny corundum inclusions (Fig. 5e). Close to these sillimanites, isolated, anhedral tiny staurolite grains (up to 0.3 mm) are also present (Fig. 5e and f). In some cases, the presence of spinel and sillimanite inclusions can be observed at the margins of corundum (Fig. 5e). In some Grt_4 (Fig. 5h), coexistence of corundum and sillimanite clusters pseudomorphing kyanite are observed in the mantle part (Fig. 5i).

Towards the rim area of Grt_4, isolated kyanite (Supplementary file 3b shows the Raman Spectrum of this kyanite) and quartz inclusions are present (Fig. 5d). In addition, coarse patches of pyrophyllite are present, in which relics of fibrolitic sillimanite could be observed (Fig. 5g). The shape of the pyrophyllite patch indicates the existence of fibrolitic sillimanite, pseudomorphing kyanite, which is a very common feature of Grt_4.

Close associations of sillimanite clusters which represent pseudomorph kyanite and isolated quartz are present from core to rim of the other side in the same garnet (Fig. 5j,k,m). Rare isolated staurolite grains are present close to quartz inclusions (Fig. 5m). However, there are no quartz inclusions in the corundum bearing portion of the particular garnet.

Hence, the presence of kyanite and/or kyanite pseudomorph + corundum ± staurolite in core to mantle areas of Grt_4 indicates the prograde reaction:

$$St => Grt + Crn + Ky + V \quad (5)$$

This may indicate that reaction (5) has taken place during prograde compression stage of the HC metasediments.

The inclusions of kyanite pseudomorph + quartz ± staurolite in the mantle to rim area and indicates that these inclusion bearing portions of the garnet have formed under quartz saturated conditions independent of reaction (5). Possible reactions in theses quartz saturated domains are referred in the discussion section.

Presence of sillimanite pseudomorphs after kyanite - quartz - staurolite from core to rim of one side in some Grt_4 indicate the reaction:

$$St + Qtz => Grt + Ky \quad (6)$$

On the other side of Grt_4, the presence of corundum together with sillimanite containing spinel inclusions can be explained by the reaction,

$$Grt + Crn => Spl + Sil \quad (7)$$

Dharmapriya et al. (2014b) concluded that reaction (7) has taken place close to peak metamorphic conditions.

During retrogression at much lower P and T, pyrophyllite has formed at the expense of fibrolitic sillimanite via the reaction,

$$Sil + Qtz + H_2O => Prl \quad (8)$$

The matrix of the studied khondalite consists of quartz saturated domains which is mainly composed of ribbon quartz, coarse-grained sillimanite, alkali-feldspars (from 0.3 up to 1 cm) as major mineral phases (Supplementary file 2n,o). Ilmenite is present as a minor constituent while zircon is present as an accessory mineral. Elongated quartz and coarse-grained sillimanite needles show a preferred orientation and define the major foliation and lineation of the rock (Supplementary file 2n). Coarse-grained, euhedral to subhedral alkali-feldspar is present within the pressure shadow of some porphyroblastic Grt_4. The tiny sillimanite inclusion bearing anhedral quartz (Supplementary file 2o) could probably result from crystallization of a melt phase during the retrogression.

4. Mineral chemistry

Mineral compositions were analyzed using a JEOL JXA8530 Field Emission Electron Probe Microanalyzers (EPMA) installed at three laboratories: (1) Department of Environmental Changes, Faculty of Social and Cultural Studies, Kyushu University, Japan, (2) Indian Institute of Science, Bangalore, India and (3) National Consortium at the University of Utrecht, Netherlands. All analyses were carried out using an accelerating voltage of 15 kV and 20 nA beam current, 1–3 μm spot size in all three laboratories. Detailed descriptions of analytical procedures followed in the three laboratories are given in Supplementary file 4.

The following section contains the mineral compositions of studied porphyroblastic garnets and their inclusion phases.

4.1. Garnet compositions

The studied garnets in Rock A (Grt_1) are mainly almandine-pyrope solid solutions, with only small amount of grossular, spessartine and andradite components (Table 1). The X_{Alm} content increased from core (~0.50) to rim (~0.58) while the X_{pyr} content gradually decreased (~0.430 at cores and ~0.370 at rims). The X_{Mg} value and Ca content vary from ~0.43 to ~0.40 and 0.18 wt.% to 0.11 wt.% respectively, from core to rim.

The garnets in Rock B (Grt_2) also exhibit mainly almandine-pyrope solid solutions (Table 1). Both X_{Alm} and X_{Pyr} contents of Grt_2 show slight variations from core to rim. However, here the X_{Alm} content decreased (~0.46 and 0.44 respectively) and X_{Pyr} (~0.45

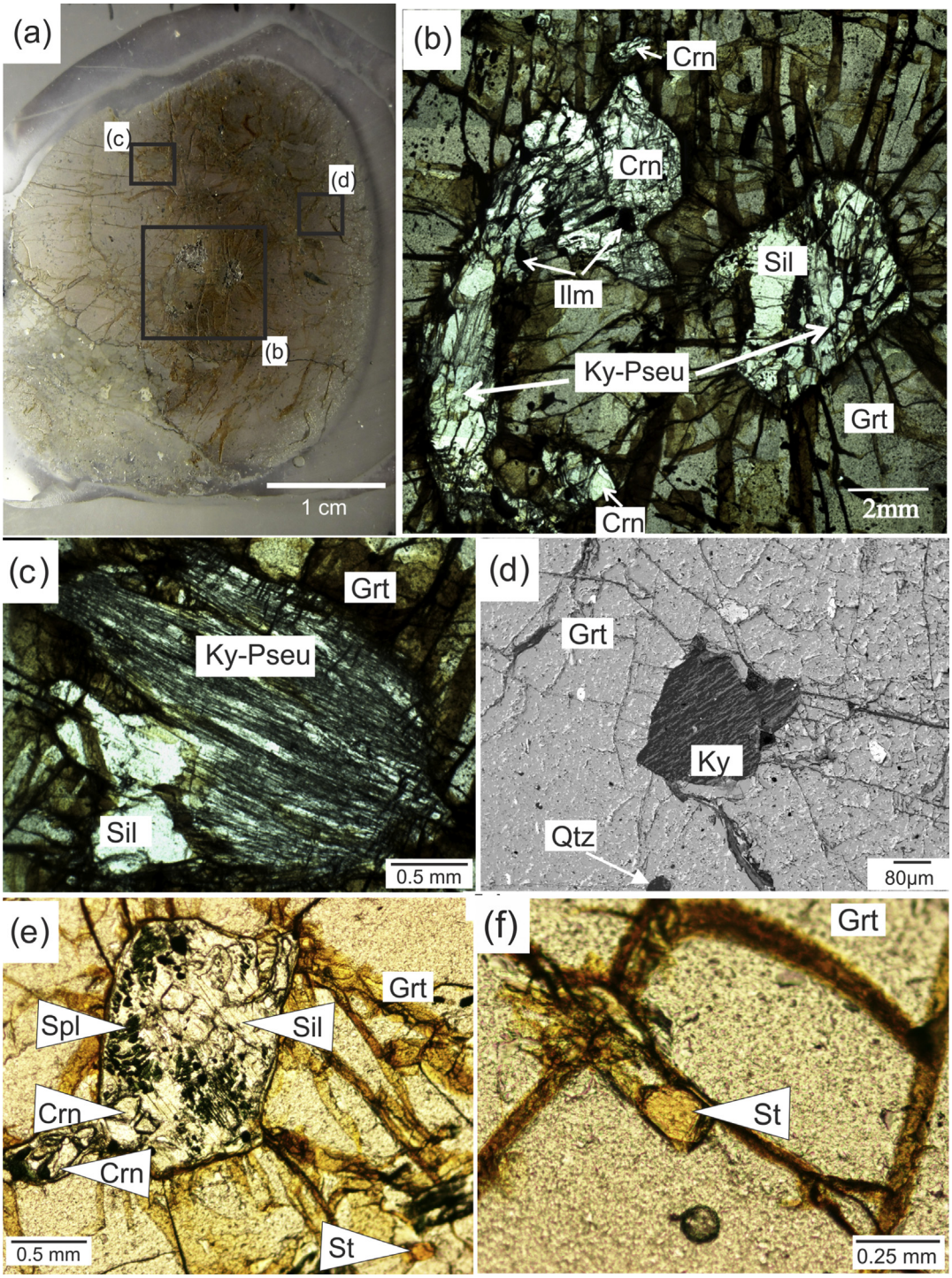

Figure 5. Petrography of Grt_4 in Rock D (images b–d show the textures of the Grt_4 of the image (a); images i–m show the textures of the Grt_4 of the image (h)). (a) A petrographic thin section showing a Grt_4 (b) as a mosaic with anhedral corundum and sillimanite clusters which pseudomorph kyanite in the core area; (b) aggregate of fibrolitic sillimanite pseudomorphing kyanite; (c) isolated kyanite grain towards the rim are. An isolated quartz grain also present close to kyanite, (e) tiny spinel inclusions and corundum inclusions in coarse prismatic sillimanite; a staurolite grain is also present in the bottom right hand side of the image; (f) an isolated staurolite grain; (g) formation of pyrophyllite towards the rim; (h) petrographic thin section of another phorphyroblastic garnet grain; (i) core existence of corundum and sillimanite clusters which pseudomorph kyanite in the mantle area; (j) tiny inclusion of quartz close to kyanite pseudomorph after sillimanite; (k) isolated cluster of sillimanite pseudomorphing kyanite; (l) close association of isolated quartz and cluster of sillimanite pseudomorphing kyanite; (m) isolated quartz, staurolite and cluster of sillimanite pseudomorphing kyanite.

and 0.48 respectively) content increased from core to rim. There is a considerable zonation of Ca content from core to rim (~1.90 wt.% and 1.00 wt.% respectively).

Similar to previous garnets, the studied garnet in Rock C (Grt_3) also exhibits mainly almandine-pyrope solid solutions (Table 1). In Grt_3 the X_{Alm} content gradually increased from core to rim (~0.46 to 0.51 respectively) while X_{Pyr} shows the opposite behavior (~0.51 to 0.45 respectively). The Ca content is approximately the same from core to rim (~0.80 wt.% and 0.70 wt.% respectively).

The garnets in Rock D (Grt_4) are mainly of almandine-pyrope solid solutions, with only small amounts of grossular, spessartine and andradite components (Table 1). The Grt_1 shows similar X_{Alm}

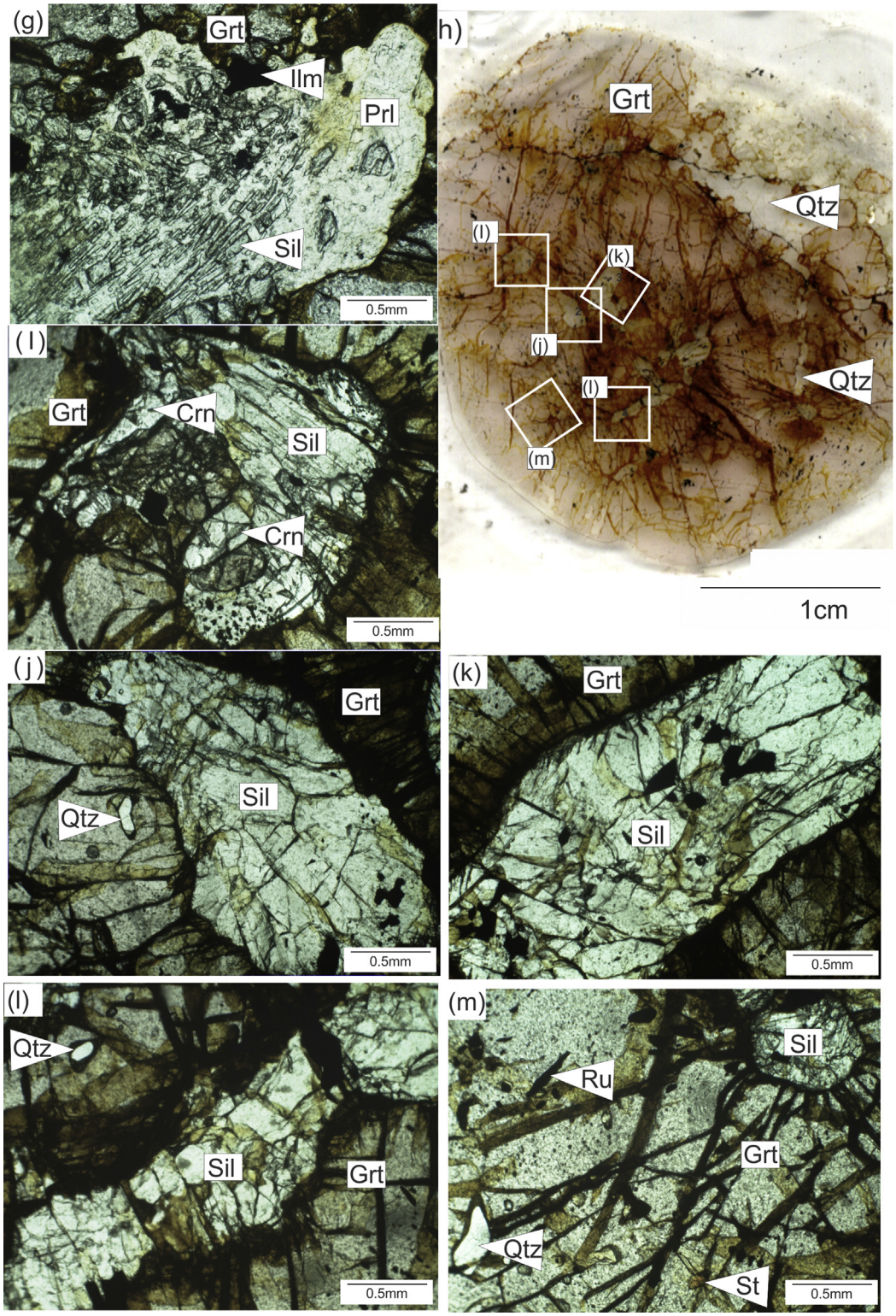

Figure 5. (*continued*)

content (~0.73) from core to rim. But the X_{Pyr} content increased (0.13 and 0.15 respectively) from core to rim. The cores of theses garnets display a relatively lower X_{Mg} value (~0.15) while rims display X_{Mg} value (~0.16). The MnO contents is ~3.6 wt.% in core compositions and ~3.2 wt.% in the rims while higher amount of Ca ~2.1 wt.% were in the core ~1.6 wt.% at the rim.

4.2. Biotite

Biotite inclusions in Grt_1, Grt_2 and Grt_3 show high Ti content (from ~5.00 to ~6.70 wt.%, Table 2). All the biotite inclusions are Mg-rich and the X_{Mg} value is relatively higher in biotite inclusions within garnet (X_{Mg} 0.74–0.78).

Table 1
Representative EPMA data of the studied garnets (major elements are in wt.%).

	Rock A			Rock B			Rock C			Rock D		
	Core	Mantle	Rim	Core	Mantle	Rim	Core	Mantle	Rim	Core	Mantle	Rim
SiO_2	39.98	39.50	39.50	40.61	40.08	40.30	40.58	39.29	39.73	36.82	36.24	36.73
TiO_2	0.05	0.00	0.05	0.05	0.00	0.02	0.02	0.02	0.00	0.04	0.03	0.03
Al_2O_3	22.28	22.43	22.03	22.64	22.89	22.46	22.69	22.43	22.43	20.98	21.09	21.10
Cr_2O_3	0.00	0.02	0.00	0.04	0.04	0.00	0.04	0.01	0.00	0.01	0.01	0.02
FeO	23.97	25.37	26.26	21.97	22.28	22.02	22.18	23.27	24.80	33.77	34.29	34.43
MnO	0.58	0.65	0.71	2.02	1.93	2.32	0.51	0.65	0.89	3.51	3.34	3.11
MgO	11.53	10.93	9.83	12.25	13.16	12.99	14.00	13.27	12.07	3.35	3.49	3.65
CaO	2.29	1.95	1.36	1.87	1.07	1.03	0.78	0.73	0.68	2.18	1.63	1.52
Na_2O	0.03	0.04	0.02	0.00	0.01	0.02	0.00	0.01	0.00	0.03	0.01	0.00
K_2O	0.00	0.00	0.02	0.00	0.00	0.00	0.00	0.01	0.00	0.00	0.00	0.00
Total	**100.71**	**100.89**	**99.78**	**101.5**	**101.45**	**101.16**	**100.80**	**99.69**	**100.60**	**100.69**	**100.13**	**100.59**
O	12	12	12	12	12	12	12	12	12	12	12	12
Si	3.005	2.984	3.024	3.013	2.974	3.000	3.005	2.968	2.992	2.958	2.933	2.952
Ti	0.003	0.000	0.003	0.003	0.000	0.001	0.001	0.001	0.000	0.002	0.002	0.002
Al	1.974	1.997	1.988	1.980	2.002	1.970	1.981	1.997	1.991	1.987	2.012	1.999
Cr	0.000	0.001	0.000	0.002	0.002	0.000	0.002	0.001	0.000	0.001	0.001	0.001
Fe	1.507	1.603	1.682	1.363	1.383	1.371	1.374	1.470	1.562	2.269	2.321	2.314
Mn	0.037	0.042	0.046	0.127	0.121	0.146	0.032	0.042	0.057	0.239	0.229	0.212
Mg	1.292	1.230	1.122	1.355	1.455	1.441	1.545	1.494	1.355	0.401	0.421	0.437
Ca	0.184	0.158	0.112	0.149	0.085	0.082	0.062	0.059	0.055	0.188	0.141	0.131
Na	0.004	0.006	0.003	0.000	0.001	0.003	0.000	0.001	0.000	0.005	0.001	0.000
K	0.000	0.000	0.002	0.000	0.000	0.000	0.000	0.001	0.000	0.000	0.000	0.000
Total cation	8.007	8.020	7.981	7.993	8.024	8.015	8.002	8.033	8.012	8.049	8.060	8.047
Fe^{3+}	0.021	0.060	0.000	0.000	0.072	0.045	0.006	0.100	0.036	0.048	0.178	0.140
Fe^{2+}	1.486	1.542	1.682	1.355	1.311	1.326	1.367	1.370	1.526	2.220	2.142	2.174
Alm	0.496	0.519	0.576	0.459	0.441	0.443	0.455	0.462	0.510	0.728	0.730	0.736
Spe	0.012	0.014	0.015	0.042	0.041	0.049	0.011	0.014	0.019	0.078	0.078	0.072
Pyr	0.431	0.414	0.372	0.449	0.490	0.481	0.514	0.504	0.453	0.132	0.143	0.148
Grs	0.052	0.034	0.138	0.061	0.013	0.015	0.017	0.006	0.009	0.044	0.017	0.017
X_{Mg}	0.46	0.43	0.40	0.50	0.51	0.51	0.53	0.50	0.46	0.15	0.15	0.16

Table 2
Representative EPMA data of biotite, staurolite, spinel, sapphirine and corundum inclusions in the studied garnets (major elements are in wt.%).

	Bt			St	Spl		Spr			Crn
	Rock A	Rock B	Rock C	Rock D	Rock A	Rock C	Rock A	Rock B	Rock C	Rock D
SiO_2	37.42	36.78	36.72	23.29	0.12	0.09	12.16	13.24	12.60	0.01
TiO_2	6.77	5.01	6.39	1.55	0.02	0.01	0.03	0.07	0.07	0.01
Al_2O_3	16.61	16.34	16.76	57.87	63.20	63.70	64.65	60.45	61.51	100.62
Cr_2O_3	0.00	0.03	0.00	0.13	0.08	0.04	0.02	0.11	0.00	0.04
FeO	9.13	9.02	9.88	11.23	19.13	14.59	7.01	9.48	9.78	0.43
MnO	0.03	0.07	0.05	0.05	0.08	0.00	0.06	0.04	0.05	0.00
MgO	15.69	18.01	16.02	2.55	14.43	15.52	16.01	16.61	15.23	0.00
CaO	0.01	0.00	0.02	0.05	0.03	0.00	0.01	0.01	0.04	0.00
Na_2O	0.47	0.09	0.42	0.00	0.02	0.00	0.03	0.04	0.00	0.00
K_2O	9.45	9.78	9.56	0.00	3.14	0.01	0.02	0.00	0.00	0.00
ZnO	0.00	0.00	0.00	1.56	3.0.14	5.59	0.00	0.00	0.00	0.00
Total	**95.58**	**95.12**	**95.82**	**98.28**	**100.26**	**99.54**	**100.01**	**100.05**	**99.29**	**101.12**
O	22	22	22	23	4	4	10	10	10	3
Si	5.419	5.367	5.336	3.230	0.003	0.002	0.722	0.796	0.763	0.000
Ti	0.737	0.549	0.698	0.162	0.000	0.000	0.001	0.003	0.003	0.000
Al	2.835	2.809	2.871	9.461	1.960	1.972	4.521	4.283	4.393	1.995
Cr	0.000	0.003	0.000	0.014	0.002	0.001	0.001	0.005	0.000	0.001
Fe	1.106	1.101	1.201	1.303	0.421	0.320	0.348	0.477	0.496	0.006
Mn	0.004	0.009	0.006	0.006	0.002	0.000	0.003	0.002	0.003	0.000
Mg	3.386	3.916	3.469	0.527	0.566	0.607	1.416	1.488	1.376	0.000
Ca	0.002	0.000	0.003	0.007	0.001	0.000	0.001	0.001	0.003	0.000
Na	0.132	0.025	0.118	0.000	0.000	0.000	0.003	0.005	0.000	0.000
K	1.746	1.820	1.772	0.000	0.001	0.000	0.002	0.000	0.000	0.000
Zn	0.000	0.000	0.000	0.160	0.061	0.108	0.000	0.000	0.000	0.000
Total cation	15.366	15.600	15.476	14.870	2.955	2.903	7.018	7.059	7.037	2.002
X_{Mg}	0.75	0.78	0.74	0.29	0.57	0.66	0.80	0.76	0.74	

4.3. Staurolite

Staurolites (Table 2) are enclosed by Grt_4 are Zn-bearing (ZnO = 1.60 wt.%) and rich in Ti (TiO_2 = 1.6 wt.%). The X_{Mg} value of the staurolite inclusions is ~0.29.

4.4. Spinel

Spinel in Grt_1 (Table 2) show ZnO content of ~3.1wt. %. The X_{Mg} value of spinel inclusions are around 0.57. Spinel in Grt_3 has relatively higher Zn content (~5.6 wt.%) while the X_{Mg} is 0.66.

4.5. Sapphirine

The composition of sapphirine in Grt_1 is very close to the end member 2:2:1 while those in Grt_2 are in between the end member compositions of 2:2:1 and 7:9:3. The X_{Mg} value of sapphirine in Grt_1 is around 0.76 while those in Grt_2 have values of about 0.80. Sapphirine in Grt_3 is also close to end member 2:2:1 with an X_{Mg} value of 0.74.

5. *P-T* calculations of garnets

Dharmapriya et al. (2015b) evaluated the *P-T* evolution of Rocks A, B and C using textural observations coupled with conventional thermobarometry. Calculations show that these rocks were metamorphosed to ~11–12 kbar around 800–850 °C during prograde stage. The rocks subsequently underwent prograde decompression with increasing temperature up to peak UHT conditions. The peak metamorphic *P-T* conditions are 900–975 °C at ~9.5–10 kbar.

Experimentally calibrated, pressure independent sapphirine-spinel geothermometry (Das et al., 2006) yielded temperature range from 820–868 °C (average 837 °C) for coexisting spinel-sapphirine pairs in Grt_1. However, it is difficult to determine the temperature conditions of the reaction (1) based on above Fe-Mg exchange thermometry, since mineral chemistry of these very tiny mineral inclusions such as sapphirine and spinel may have been undergone modification due to intense chemical diffusion under UHT peak metamorphic conditions and subsequent re-equilibration during the retrogression.

Dharmapriya et al. (2015b) showed that Ti-in biotite thermometer yielded the prograde temperature up to 845 °C for biotite inclusions in Grt_1. From melting experiments of natural metapelites under fluid-absent conditions, Vielzeuf and Holloway (1988) pointed out that the reaction (2) has taken place under the minimal *T* of ~860 °C. Since the Ti content of the biotite inclusions in garnet of the Rock A is up to 7 wt.%, the breakdown of the biotite could have taken place at very high temperature conditions. Hence, it is logical to speculate that reaction (1) had taken place prior to the reaction (2) during the prograde decompression with increasing temperature of the Rock A.

The *P-T* conditions of the inferred reaction (3) in Rock B can be evaluated by the existing experimental results. Based on experimental investigations, Schreyer (1988) suggested that pure Mg-staurolite is stable at $P > 14$ kbar and $T > 710$–760 °C in the MASH ($MgO–Al_2O_3–SiO_2–H_2O$) system. Later Fockenberg (1998) reported the stability of Mg-staurolite at *P–T* conditions of 12–66 kbar and 608–918 °C. Unfortunately the experimental results observed from pure Mg-staurolite are difficult to apply directly to the natural rocks (Kelsey et al., 2006; Tsunogae and van Reenen, 2011). In contrast, Sato et al. (2010) reported high-*P-T*, experiments of staurolite with moderate X_{Mg} (= 0.7–0.5) at 12–19 kbar and 850–1050 °C. As mentioned in the section 3.2, due to occurrence of staurolite with X_{Mg} ~0.50 in the central HC close to sampling locality of Rock B, the reaction (3) could have taken place at *P-T* of ~11–12 kbar and ~820–850 °C which is the derived prograde *P-T* condition of the Rock B (see Dharmapriya et al., 2015b). Hence the Ti-rich biotite (up to 5.00 wt.%) could probably break down via reaction (2) just after the reaction (3) during the prograde decompression with increasing temperature of the Rock B.

The biotite dehydration reaction (2) and (4) in Rock C could also have taken place contemporaneously during the prograde decompression. Dharmapriya et al. (2015a) showed evidence for formation of garnet via the prograde dehydration reaction (2) in a corundum bearing pelitic granulite. Core area of some of those garnets contains biotite, sillimanite and quartz inclusions. Due to the presence of spinel inclusions at the rim of the same garnet and absence of quartz at the garnet rim or in the matrix of the rock, these authors argued that the garnet rim could have formed after the complete consumption of quartz via reaction Bt + Sil => Grt + Spl + Kfs + melt during the prograde decompression with increasing temperature. However, in the Rock C, formation of a vast area of Grt_3 (from core to rim) is a result of the reaction (2). The reaction (4) represents only at the mantle area in one side of the Grt_3.

Authors have further evaluated the *P-T* evolution of Rock D using textural observations coupled with pseudosections, petrogenetic grids and conventional thermobarometry and found that the Rock D has reached ~11 kbar at 780 °C during prograde metamorphism. Subsequently, it has undergone a decompression stage with increasing temperature, reaching peak *T* of ~900 °C at ~9 kbar. Using petrogenetic grids, numbers of workers (e.g., Hiroi et al., 1994) have shown that reaction (5) had taken place prior to reaction (6).

The prograde conditions existed in minor silica-deficient domains of Grt_4 of Rock D were evaluated using pseudosections (using Perplex_X_07 after Connolly, 2005) based on calculated local bulk rock compositions for the silica-deficient domain of Grt_4 using estimated ratios among garnet, kyanite, corundum and staurolite (Table 3). Based on textural observations (Fig. 5), it is inferred that all corundum grains enclosed by garnet are produced as a result of staurolite breakdown via reaction (5). This is a reaction with changes in minor elements (e.g., minor Ti enrichment in staurolite and some Mn and Ca dilution in garnet). The modal abundances of Grt_4, staurolite and kyanite prior to the corundum formed by breakdown of staurolite, were recalculated (Table 3). The results suggest that some kyanite was already present before staurolite started to breakdown. The amount of H_2O was added stoichiometrically equivalent to that ideally resided in the staurolite, which is likely to have escaped the system along the prograde path. Pseudosections were calculated in FMAS and FMAS systems at $X_{Mg} = 0.15$ which was the X_{Mg} of Grt_4. Though staurolite has $X_{Mg} = 0.29$, the effect of X_{Mg} of staurolite was neglected as the obtained staurolite volume in Grt_4 is ~1%. The used composition have labeled in each pseudosection. Fig. 7a shows the model-pseudosection (where SiO_2 is 38.01 mol%) for this small reaction domain, assuming local equilibrium (e.g., Stüwe, 1997) within the Grt_4 porphyroblast hosting the reaction domain. This shows that the *P-T* field for the inferred staurolite breakdown reaction is largely consistent with the FASH ($FeO–Al_2O_3–SiO_2–H_2O$) end-member reaction, but has shifted to higher *P* and *T*. Thus, the results indicate that staurolite broke down to Grt + Ky + Crn + V (bold field) between 8 and 12 kbar at temperatures between 730 and 800 °C (Fig. 6a). It is likely that H_2O was lost from the assemblage at this stage.

Since the assemblage outside the Grt_4 porphyroblast contains abundant quartz and it lacks corundum, it is deduced that garnet

Table 3
Reaction and mass balance of staurolite breakdown reaction in FASH.

	Grt	Ky	Crn	H_2O	St
FASH end-member system (molar)					
FeO	3	0	0	0	4
Al_2O_3	1	1	1	0	9
SiO_2	3	1	0	0	7.5
H_2O	0	0	0	1	2
Reaction coefficient	1.333	3.5	4.167	2	−1
Molar V	11.526	4.404	2.545		44.88
Observed mode (V %)	60	25	14		1
Observed mode (molar)	5.2	5.7	5.5		0.02
Original mode (molar)	3.45	1.06	0		1.34
Normalised	0.23	0.07	0		0.09

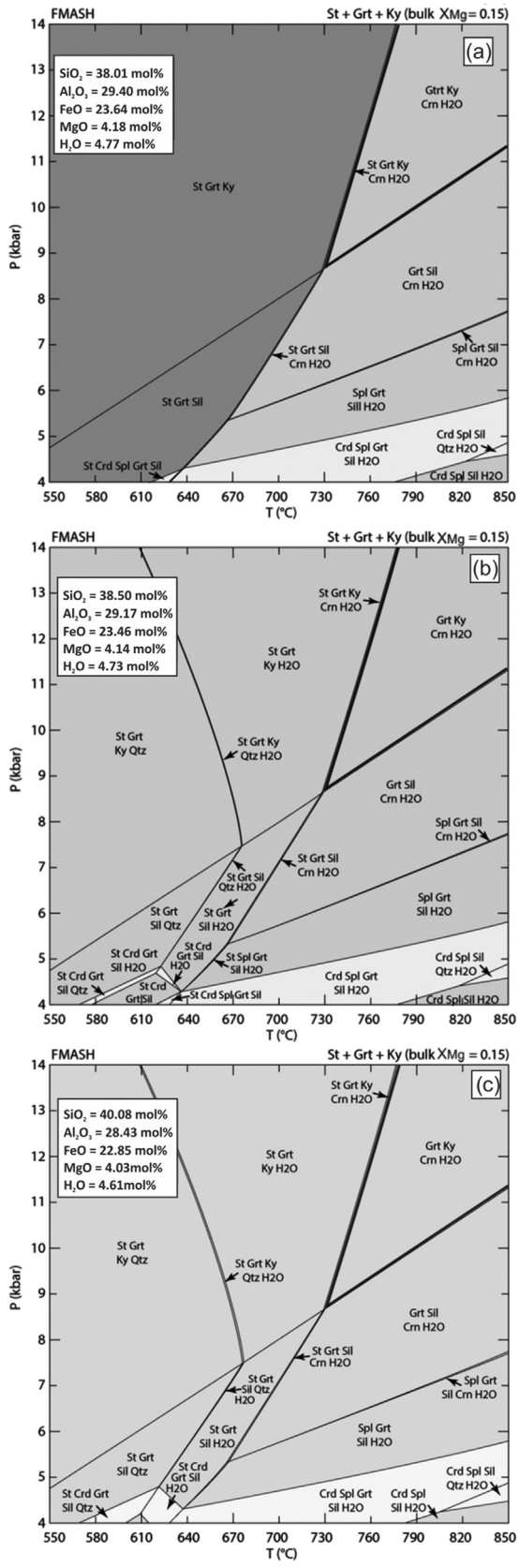

Figure 6. *P-T* pseudosection represented in FMASH system using local rock compositions calculated from mineral analyses and estimated abundances for specific garnet Grt_4 in Rock D under different bulk SiO_2 content: (a) at SiO_2 = 38.01 mol%, (b) SiO_2 = 38.5 mol%, (c) SiO_2 = 40.8 mol%.

originally enclosed some quartz. Hence, another two pseudosections (Fig. 6b and c) were calculated after adding some SiO_2 (at 38.5 and 40.08 mol%) to investigate a possible earlier path leading to quartz depletion. It turns out that, above 6 kbar, the resulting diagram (Fig. 6b and c) do not change even more SiO_2 is added. Thus the results show that reaction (5) operated between 8 and 12 kbar at temperatures above 730 °C. These calculations are typical with the obtained result from pseudosections constructed under the pre-melting, of which original rock composition was calculated through stepwise re-integrations of melt into the residual XRF composition, showing that the rock has reached >10 kbar at 750–775 °C during prograde metamorphism (Dharmapriya et al., accepted).

6. Discussion

6.1. A model for the incorporation of silica-saturated and silica-deficient microdomains in single garnet grains

Silica-saturated and silica-deficient portions in the same garnet can result in different ways. One possibility is the consumption of quartz during the progress of garnet formation reactions, which could lead to quartz depletion (e.g., Alvarez-Valero and Kriegsman, 2010; Dharmapriya et al., 2015a). Subsequent garnet-producing reactions may lead under the silica-deficient garnet rims (e.g., Dharmapriya et al., 2015a). This mechanism generally leads to a concentric zonation pattern with silica-saturated domains in the garnet core and silica-deficient domains in the garnet mantle to rim.

In a second mechanism, quartz can be incorporated into garnet by crystallization of a melt inclusion (Sawyer, 2001; Harley, 2008). Even a dehydration melting reaction under silica-deficient conditions can produce a melt phase that later precipitates forming quartz. This mechanism can produce a random distribution of quartz-bearing and quartz-deficient domains in garnet.

Here, we discuss an alternative mechanism to form silica-saturated and silica-deficient domains in single garnet grains in an alternating pattern that may explain some contrasting observations. In addition, it is essential to evaluate the *P-T* conditions at which the particular silica-saturated and silica-deficient mineral reactions were taken place, due to the fact that silica-saturated granulites are generally indicative of high to extreme temperature metamorphism (Kelsey and Hand, 2015). Such silica-saturated granulites may contain mineral assemblages, which are diagnostic to ultrahigh temperature conditions (e.g., Harley, 2008; Kelsey and Hand, 2015). In contrast, the stability of silica-deficient granulites usually expands to lower temperatures than that for silica-saturated assemblages. Further, there are only few localities of silica-deficient granulites globally, which record temperatures less than 900 °C (e.g., Prakash and Sharma 2008, 2011; Sharma and Prakash, 2008; Nasipuri et al., 2009; Prakash et al., 2013; Prakash and Singh, 2014).

6.1.1. Formation of Grt_1

The distribution of inclusion phases in Grt_1 reveals that high Al/low-Si reaction (1) has contributed to the growth of core areas of some garnet grains and rim areas of some other grains. Similarly, high-Al/high-Si reaction (2) produced mantle to rim areas of some garnet grains, but core to mantle areas of some other grains. Hence, we consider that Grt_1 grains have grown across alternating microdomains with different effective bulk compositions, namely high-Al/low-Si versus high-Al/high-Si microdomains.

However, *P-T* estimations indicated that the reaction (1) could probably have taken place prior to the reaction (2) during the prograde decompression. Thus, it is more logical to explain the high Al/low-Si reaction (1) around the core and high-Al/high-Si reaction (2) from mantle to rim of the same garnet grain. Nevertheless, the

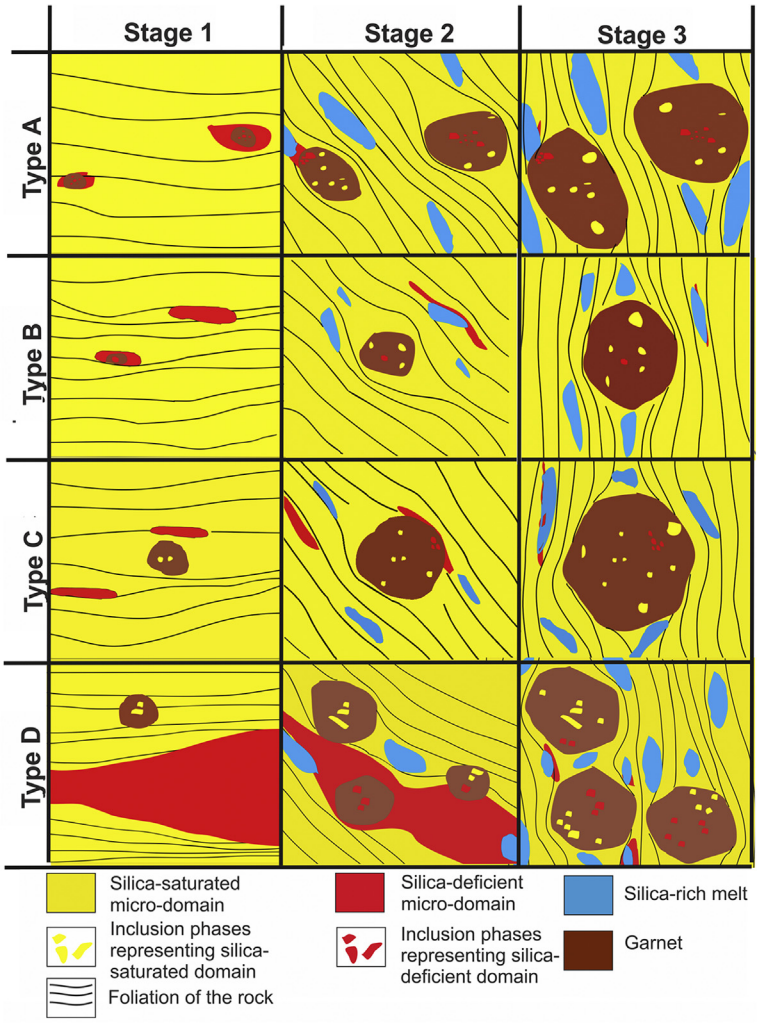

Figure 7. A cartoon illustrating the evolution of porphyroblastic garnets across alternating silica-saturated and silica-deficient microdomains. See the rotation of the foliation of each rock during the progress of the garnet growth.

presence of high-Al/high-Si reaction (2) from core to rim of one side of the garnet and high Al/low-Si reaction (1) in the rim area of other side of the same garnet revealed that the core and mantle area of the particular garnet is younger than the rim area of the same garnet represented by the reaction (1).

6.1.2. Formation of Grt_2

Inclusions of kyanite + sapphirine in the core areas of Grt_2, indicated that garnet started growing via reaction (3) in high-Al/low-Si domains, followed by reaction (2) in high-Al/low-Si mantle to rim areas.

6.1.3. Formation of Grt_3

The inclusion phases indicate that most of Grt_3 has formed via reaction (2) which is typical for high-Al/high-Si domains. However the presence of sillimanite + sapphirine and spinel + sillimanite without quartz as inclusions indicates that some high-Al/low-Si microdomains were present where garnet grew via reaction (4). Hence, Grt_3 has also grown across microdomains with different compositions during prograde metamorphism.

6.1.4. Formation of Grt_4

Inclusion phases of Grt_4 reveal that this garnet type also grew across microdomains with different bulk compositions. The incorporation of sillimanite pseudomorphs after kyanite accompanied by quartz ± staurolite in core to rim on one side of a garnet (Fig. 5l–n) indicates that this side of the garnet has formed in a high-Al/high-Si microdomain via reaction (6). Sillimanite pseudomorphs after kyanite + corundum toward the mantle on the other side in the same garnet (Fig. 5k) indicated that the particular portion of the garnet has formed via reaction (5) in a high-Al/low-Si micro domain. In the FASH chemical system (e.g., Hiroi et al., 1994), reaction (6) operates at lower *P-T* conditions than reaction (5).

In contrast, core to mantle areas of some other Grt_4 with corundum and sillimanite pseudomorphs after kyanite ± staurolite indicated that the evolution of those garnets had taken place via the reaction (5) at aluminum-rich, silica-deficient microdomains. However, the presence of quartz, kyanite and/or kyanite-pseudomorphs ± staurolite ± K-feldspar towards the mantle to rim area of some Grt_4 (where corundum, kyanite-pseudomorph ± staurolite present at the core) indicates that the mantle to rim area of these garnets had formed at Al-rich, silica-saturated microdomains and hence independent from reaction (5).

One possibility is that the quartz inclusion bearing portions of Grt_4 could have formed via reaction (6). Though, in the FASH chemical system (e.g., Hiroi et al., 1994) the reaction (6) takes place relatively at lower *P-T* conditions prior to reaction (5). However, Fockenberg (1998) suggested that end-member Mg-staurolite is

stable at very wide range of *P-T* conditions of pressures from 12 to 66 kbar and temperatures ranging from 608 to 918 °C. Ti content can also shift the stability field of staurolite to relatively higher temperature conditions (e.g., Raase and Schenk, 1994). However, in the present case, the X_{Mg} content of staurolite in both silica saturated and deficient domains are approximately similar (~0.30). Available experimental and thermodynamic studies of staurolite suggest that typically Fe-rich staurolite becomes unstable above the amphibolite facies resulting the progress of the ((K)FMASH) continuous reactions St + Ms + Qtz => Grt + Bt + Ky + H_2O or the reaction (6) at ~700 °C (e.g., Spear and Cheney, 1989; Tsunogae and van Reenen, 2011). However, both reactions take place prior to the reaction (5) in *P-T-t* space. Hence the possibility is that the garnet formation could initiate in Al-rich but quartz-deficient microdomains and, then continue into Al-rich and quartz-saturated microdomains. Further, the core area of the garnet may also be formed in Al-rich and quartz-deficient microdomains. In such a case, the quartz inclusion-bearing mantle to rim area of the garnet is relatively older than the corundum inclusion bearing core.

6.2. Existence of silica-saturated and silica-deficient microdomains in metasediments during the prograde metamorphism

Locally existing of macro to micro scale silica-saturated and silica-deficient bulk compositional domains are reported in metasediments from numerous medium to high grade metamorphic terrenes (e.g., Powell and Vernon, 1979; Adjerid et al., 2008, 2013; Harley, 2008; Jiao et al., 2013; Dharmapriya et al., 2015a). For an example, Dharmapriya et al. (2015a) reported macro-scale compositional differences between silica-saturated and silica-deficient rock domains from the HC. Authors argued that these compositional domains may reflect a primary heterogeneity in the sediment during deposition. A number of workers reported evidence for the presence of closely associated silica-saturated and silica-deficient microdomains in medium grade to HT/UHT metamorphic rocks (Powell and Vernon, 1979; Adjerid et al., 2008, 2013; Jiao et al., 2013; Kelsey and Hand, 2015). Jiao et al. (2013) reported existence of silica-saturated and silica-deficient microdomains in HT granulites of Khondalite belt, North China Craton. Those authors showed textural evidence for various inclusion bearing garnets and different garnet break down reactions at silica-saturated and silica-deficient microdomains in the same rock. Further, Adjerid et al. (2013) reported textural evidence for silica-saturated and silica-deficient reactions occurring in close microdomains at UHT granulites of Khanfous area in Ouzzal metacraton, Hoggar, Algeria. Silica-saturated and silica-deficient domains can result in metasedimentary rocks by processes such as metamorphic differentiation (e.g., Fletcher, 1977), formation of differentiated crenulated cleavages (e.g., Williams, 1972; Granath, 1980), crystallization of silica saturated melt pods in silica-deficient rocks (e.g., Harley, 2004, 2008), local influxes of silica rich fluid phase into silica deficient rock (e.g., Leite et al., 2009) and existence of original compositional heterogeneity in protolith sedimentary rocks which represent silica-saturated and silica-deficient domains (e.g., Dharmapriya et al., 2015a). Textual evidence indicates that genesis of all studied garnets incorporate inclusion phases representing distinct silica saturated and silica-deficient dehydration reactions which could contribute to progress of garnet formation around upper amphibolite (e.g., Grt_4) to amphibolite to granulite facies transition (e.g., Grt_1, Grt_2 and Grt_3). In other words, garnets have grown across different effective bulk compositional microdomains which probably existed up to amphibolites facies conditions during the prograde evolution. Therefore, one possibility is to consider that the silica-saturated and deficient microdomains in Grt_1 to Grt_4 probably represent heterogeneous compositional layers such as paleobeddings/laminations which perhaps have occurred as few centimeter to millimeter in thickness in the precursor sediments. Conversely, differentiated crenulated cleavages during prograde metamorphism may also cause existence of such silica-saturated and silica-deficient domains.

Existence of various millimeters to few centimeters scale alternate compositional lamellae due to sedimentary beddings or laminations is a common feature of sedimentary rocks. The bulk chemical compositions (such as Si, Fe and Al content) of those individual lamella can vary according to the nature of deposited sediments. As an example, Emiliani (1992) reported banded iron formations consisting of laminated layers of iron-rich/silica-poor and iron-poor/silica-rich intervals. Sedimentary laminations, beddings and typical structures of sedimentary rocks such as cross-bedding and graded bedding may be preserved in low to medium grade metasedimentary rocks (Hacker and Goodge, 1990; Bucher and Grapes, 2011). Unfortunately, it is often impossible to recognize paleobedding of protolith sediments in high grade metamorphic rocks (e.g., Passchier and Trouw, 1996). Occasionally, preservation of relict paleobedding of protolith sediments in highly deformed granulite facies rocks has also rarely been reported (e.g., Touret, 1965; Perera, 1994; Kehelpannala, 1997, 2003). Perera (1994b) reported evidence for preservation of paleo cross-bedding in granulite facies rocks in the HC. Kehelpannala (1997, 2003) reported evidence for preservation of paleo bedding in metasediments from the WC close to HC-WC inferred tectonic contact. Further, Kehelpannala (2003) argued that some of the metasedimentary rocks of the HC contain modified primary-sedimentary beddings (paleobedding), which may have resulted from strong deformation and metamorphism of a sequence of sandstone, pelites and semi-pelite of protolith sediments. Touret (1965) reported preservation of extremely delicate structures such as flysch-type banding or cross-bedding in southern Norway granulite domain.

There are number of workers (e.g., Voll and Kleinschrodt, 1991; Kleinschrodt, 1994; Kröner et al., 1994b; Kehelpannala, 1997, 2003) who suggested a phenomena of strong flattening of original sedimentary sequence of the HC at the lower crustal level. Kröner et al. (1994b) argued that original supracrustal sequence in the Highland sedimentary basin were subjected to folding, thrusting and strong flattening while transporting into the lower crust during the final stages of continental collision around Sri Lanka, simultaneous with assembly of Gondwana. Hence, it is reasonable to argue that the local existence of millimeter to micrometer scale Al-rich silica-saturated and Al-rich silica-deficient lamella during the prograde evolution, which were present as few centimeter to millimeter scale bedding or laminations prior to strong flatting event of original sedimentary protoliths.

Alternatively, such Al-rich silica-saturated and Al-rich silica-deficient microdomains could be present during prograde metamorphism due to existence of differentiated crenulation cleavage which is a common type of cleavage in multiply-deformed, intermediate to high-grade metapelitic rocks (Bell and Cuff, 1989; Williams et al., 2001). Several workers (e.g., Schoneveld, 1977; Bell and Cuff, 1989; Kim and Bell, 2005; Sharib and Bell, 2011) have reported evidence for genesis of garnet porphyroblasts across the compositionally different, differentiated crenulation cleavages. Further, existence of quartz-rich and quartz-deficient micro domains across the differentiated crenulation cleavages have also reported in the literature (e.g., Williams, 1972; Fletcher, 1977; Granath, 1980).

The next questions are, if the above garnets (Grt_1–Grt_4) have grown across different effective bulk compositional microdomains: (1) Why the evidence for continuation of theses different effective bulk compositional micro-domains is absent in the matrix? (2) Why the garnets do not show chemical zonation at silica-saturated and silica-deficient minerals bearing domains?

6.3. Disappearance of compositional domains in the matrix

The answer to the first question above is the high temperature associated multiple deformation history of the Highland Complex, which could probably obliterate the evidence of the existence of different compositional lamellae in the rock. Number of workers (e.g., Berger and Jayasinghe, 1976; Yoshida et al., 1990; Kehelpannala, 1991, 1997; Kriegsman, 1991, 1994) suggested that the Sri Lankan basement suffered multiple deformation events.

Most of above workers (Berger and Jayasinghe, 1976; Kriegsman, 1991, 1994; Kehelpannala, 1997) have suggested that the present major gneissic foliation and major lineation (S_2 and L_2 respectively) in the HC granulites have been resulted during the D_2 deformation event simultaneously with the peak metamorphism of HC during assembly of Gondwana (e.g., Kröner et al., 2003; Kehelpannala, 2004). The evidence for early foliation (S_1) represented in some of mineral inclusions as trails indicating a well developed crenulation, resulted during D_1 deformation event in the host garnets (Yoshida et al., 1990; Kehelpannala, 1991, 1997; Kriegsman, 1991) and some others, mainly sillimanite needles, display an internal folding or crenulations (Kehelpannala, 1991; Kriegsman, 1991; Kröner et al., 1994b). Presence of mineral lineation, which is oblique to major matrix lineation L_2 in some garnets, could represent the early mineral lineation L_1 (Yoshida et al., 1990; Kriegsman, 1991, 1994; Kehelpannala, 1997). D_2 deformation event may have had two main phases (Kehelpannala, 1997): the first phase is less strong and resulted in an early phase producing crenulation folds (some of which are now included in garnet porphyroblasts) and small scale crenulation fold hinges found in metapelites, and later phase is the strongest ductile deformation caused the formation of strong stretching lineation (L_2) and prominent foliation (S_2).

Suggested D_1 deformation, which predates the peak granulite facies metamorphism in the HC, has been interpreted as being due to some early tectonic event. Some rare textural evidence preserved in garnet porphyroblasts indicates that the HC metasediments have entered from sillimanite stability field to kyanite stability field during prograde evolution probably due to the crustal thickening (Raase and Schenk, 1994; Malaviarachchi and Takasu, 2011a; Dharmapriya et al., 2014b, 2015b).

All of our studied garnets are formed by dehydration reactions during prograde metamorphism. Hence growths of theses garnets have taken place under D_1 and early stage of D_2 events, which took place prior to peak metamorphism. Therefore, during the D_1 event, the crustal thickening may have caused strong flattening and transport of metasediments into the lower crust. During this crustal thickening event, the original sedimentary sequence in the HC have probably been continuously destroyed (Kröner et al., 1994b; Kehelpannala, 1997, 2003). Although the original sequence of the sedimentary units could be destroyed by tectonic stresses, there is a tendency to preserve original palaeobeddings/laminations of the sediment sequence in the macro to micro scale (e.g., Perera, 1994; Kehelpannala, 1997, 2003).

There is sufficient evidence in studied Rock A, C and D for rotation of the foliation during the prograde evolution. The mantle area of Grt_1 contains rotated crenulation lineation demarcated by biotite and tiny sillimanite needles (Fig. 2b–d), which is oblique to the major matrix lineation of the rock. In Rock C as well, some of the garnet contains rotated crenulation lineation demarcated by sillimanite needles (Supplementary file 2g), which is oblique to the major matrix lineation of the rock. In Rock D, Type 1 garnet contains mineral lineation, which is demarcated by preferred oriented quartz grains are now oblique to major lineation L_2 in the rock matrix (Supplementary file 2i,j). Further, existence of curved quartz grains in core to mantle of garnet (Type 3; Supplementary file 2l) also provides evidence for rotation of the foliation during prograde metamorphism.

However, at the late stage of the D_2 deformation (Kehelpannala, 1997), the original sedimentary sequence probably have been destroyed and reworked due to strong tectonic stresses and associated granulite facies metamorphism. Estimated peak metamorphic *P-T* conditions of all of above studied rocks are 9–10 kbar and 900–975 °C. However, even under such higher temperature conditions a considerable amount of melt can be produced, as clearly seen by field and textural evidence (e.g., existence of in-situ melts in the UHT granulites in the HC) coupled with pseudosection calculations (e.g., Dharmapriya et al., 2015a,b, 2016). Some of these generated melt fraction could escape from the system making considerable changes in the bulk chemical composition of the ordinal rock. Remaining fraction of melt phases may have contributed to rework the compositions of the original rock in macro to micro scales. Further, loss of some melt phases from the system and crystallizations of new minerals from the existing melt phases during cooling after peak metamorphism could also change the original matrix structures and compositions in the studied pelitic granulites. In this context, the representative illustration interpreting the formation of various garnet grains from Grt_1 to Grt_4 is shown in Fig. 7.

6.4. Chemical homogenization of the garnets

The absence of compositional difference across the garnet in silica-saturated and silica-deficient mineral bearing domains could be due to the self-diffusion of the garnet at HT to UHT metamorphism. Further, growth zoning of garnet are frequently obliterated in high-grade garnet due to volume diffusion (Blackburn, 1969; Grant and Weiblen, 1971; Tracy et al., 1976; Yardley, 1977; Tuccillo et al., 1990; Fernando et al., 2003). Since the rates of self-diffusion of cations in silicates commonly increase exponentially with temperature (Yardley, 1977), the studied garnets could lead to chemical homogenization across the garnet grain-profile in quartz saturated and quartz deficient mineral bearing domains.

7. Conclusions

The textural evidence of the studied garnets indicates that their evolution has taken place via different dehydration reactions during prograde metamorphism. These dehydration reactions have taken place in silica-saturated and silica-deficient microenvironments of the studied rocks. Due to incorporation of mineral inclusions, which represent both silica-saturated and silica-deficient domains in same garnets, we speculate that these garnets have continued to grow across different effective bulk compositional microdomains. Due to strong ductile deformation-associated UHT metamorphism, metamorphic differentiation and crystallization of in-situ melt, the existing compositional microdomains may have disappeared and modified resulting in more homogeneous matrix within the rocks. The absence of compositional difference across the garnet grown in silica-saturated and silica-deficient domains could be due to the chemical homogenization via self diffusion of elements at high to UHT metamorphism.

Acknowledgements

Authors are grateful to the National Research Council (NRC) of Sri Lanka (Grant Nos. 11-180 and 15-089) and the Indo-Lanka Joint Grant from the Ministry of Technology and Research, Sri Lanka (MTR/TRD/AGR/3/1/04) for funding this project. P.L.D. acknowledges a Martin fellowship to work at the Naturalis Biodiversity Center, Leiden, Netherlands. L.M.K. acknowledges support by the Stichting Dr Schürmannfonds, Grant Nos. 88/2012, 94/2013 and 101/2014. Profs. M. Santosh and H.M. Rajesh are thanked for the

editorial work and valuable comments and suggestions to improve this manuscript. Two anonymous reviewers are thanked for the detailed and constructive comments and suggestions, which improved early versions of this manuscript. We also thank to Dr. Lily Wang, for her excellent editorial assistance. P.L.D appreciates Mr. Hans de Groot and Dr. Hanco Zwaan at the Naturalis Biodiversity Center, Leiden, Mr. Anil Kaushik, Dr. George Matthews, Dr. Ishwar Kumar, Dr. Vinod Samuel, Miss. P.V. Thanooja and Miss T.G. Athira at the Indian Institute of Science, Bangalore, and Mr. P. Kitano, Dr. T. Adachi and Dr. N. Nakano at Kyushu University for analytical support. Authors kindly thank Mr. O. K. S. Opatha and Miss. Thilini Harischandra of the National Institute of Fundamental Studies, Kandy for preparation of thin sections.

Appendix A. Supplementary data

Supplementary data related to this article can be found at http://dx.doi.org/10.1016/j.gsf.2016.11.008.

References

Adjerid, Z., Ouzegane, K.H., Godard, G., Kienast, J.R., 2008. First report of ultrahigh-temperature sapphirine + spinel + quartz and orthopyroxene + spinel + quartz parageneses discovered in Al-Mg granulites from the Khanfous area (In Ouzzal metacraton, Hoggar, Algeria). In: The Boundaries of the West African Craton, vol. 297. Geological Society, London, Special Publications, pp. 147–167.

Adjerid, Z., Godard, G., Ouzegane, K.H., Kienast, J.R., 2013. Multistage progressive evolution of rare osumilite-bearing assemblages preserved in ultrahigh-temperature granulites from In Ouzzal (Hoggar, Algeria). Journal of Metamorphic Geology 31, 505–524.

Ague, J.J., James, O., Eckert, J., 2012. Precipitation of rutile and ilmenite needles in garnet: implications for extreme metamorphic conditions in the Acadian Orogen, U. S. A. American Mineralogist 97, 840–855.

Ague, J.J., Carlson, W.D., 2013. Metamorphism as Garnet Sees It: the kinetics of nucleation and growth, equilibration, and diffusional relaxation. Elements 9, 439–445.

Alvarez-Valero, A.M., Kriegsman, L.M., 2010. Chemical, petrological and mass balance constraints on the textural evolution of pelitic enclaves. Lithos 116, 300–309.

Bell, T.H., Cuff, C., 1989. Dissolution, solution transfer, diffusion versus fluid flow and volume loss during deformation/metamorphism. Journal of Metamorphic Geology 7, 425–447.

Berger, A.R., Jayasinghe, N.R., 1976. Precambrian structure and chronology in the Highland Series of Sri Lanka. Precambrian Research 3, 559–576.

Blackburn, W.H., 1969. Zoned and unzoned garnets from the Grenville Gneisses around Cananoque, Ontario. Canadian Mineralogists 9, 691–698.

Bolder-Schrijver, L.J.A., Kriegsman, L.M., Touret, J.L.R., 2000. Primary carbonate/CO_2 inclusions in sapphirine-bearing granulites from central Sri Lanka. Journal of Metamorphic Geology 18, 259–269.

Braun, I., Kriegsman, L.M., 2003. In: Yoshida, M., Windley, B.F., Dasgupta, S. (Eds.), Proterozoic crustal evolution of southernmost India and Sri Lanka. Geological Society London, Special Publications, vol. 206, pp. 169–202.

Bucher, K., Grapes, R.H., 2011. Petrogenisis of metamorphic rocks and minerals, and principles of spectroscopy, in manual of remote sensing. Remote Sending of the Earth Science 3, 3–58.

Caddick, M.J., Kohn, M.J., 2013. Garnet: witness to the evolution of destructive plate boundaries. Elements 9, 427–432.

Connolly, J.A.D., 2005. Computation of phase equilibria by linear programming: a tool for geodynamic modelling and its application to subduction zone decarbonation. Earth and Planetary Science Letters 236, 524–541.

Cooray, P.G., 1994. The precambrian of Sri Lanka: a historic review. In: Raith, M., Hoernes, S. (Eds.), Tectonic Metamorphic and Isotopic Evolution of Deep Crustal Rocks, With Special Emphasis on Sri Lanka. Precambrian Research vol. 66, pp. 3–18.

Das, K., Fujino, K., Tomioka, N., Miura, H., 2006. Experimental data on Fe and Mg partitioning between coexisting sapphirine and spinel: an empirical geothermometer and its application. European Journal of Mineralogy 18, 49–58.

Dharmapriya, P.L., Malaviarachchi, S.P.K., Galli, A., Su, Ben-Xun, Subasinghe, N.D., Dissanayake, C.B., Nimalsiri, T.B., Zhu, B., 2014a. *P–T* evolution of a spinel + quartz bearing khondalite from the Highland Complex, Sri Lanka: implications for non-UHT metamorphism. Journal of Asian Earth Sciences 95, 99–113.

Dharmapriya, P.L., Malaviarachchi, S.P.K., Subashighe, N.D., Dissanayake, C.B., 2014b. *P-T* evolution of garnet-sillimanite granulites with corundum inclusions from the Highland Complex, Sri Lanka. In: Proceedings of the 30th Annual Sessions Geological Society of Sri Lanka 28th Feb. 2015 Colombo, Sri Lanka.

Dharmapriya, P.L., Malaviarachchi, S.P.K., Galli, A., Su, Ben-Xun, Subasinghe, N.D., Dissanayake, C.B., 2015a. Rare evidence for formation of garnet + corundum during isobaric cooling of UHT metapelites: new insights for retrograde P-T trajectory of the Highland Complex, Sri Lanka. Lithos 220, 300–317.

Dharmapriya, P.L., Malaviarachchi, S.P.K., Santosh, M., Tang, Li, Sajeev, K., 2015b. Late-neoproterozoic ultrahigh-temperature metamorphism in the Highland Complex, Sri Lanka. Precambrian Research 271, 311–333.

Dharmapriya, P.L., Malaviarachchi, S.P.K., Sajeev, K., Zhang, C., 2016. New LA-ICPMS U-Pb ages of detrital zircons from the Highland Complex: insights into Late Cryogenian to Early Cambrian (ca. 665–535 Ma) linkage between Sri Lanka and India. International Geology Review 58, 1856–1883.

Dharmapriya, P.L., Malaviarachchi, S.P.K., Kriegsman, L.M., Galli, A., Sajeev, K. and Zhang, C. New constraints on the *P-T* path of HT/UHT metapelites from the Highland Complex of Sri Lanka, Geoscience Frontiers, Accepted.

Emiliani, C., 1992. Planet Earth: Cosmology, Geology, and the Evolution of Life and Environment. Cambridge University Press, New York.

Faulhaber, S., Raith, M., 1991. Geothermometry and geobarometry of high grade rocks: a case study on garnet pyroxene granulites in southern Sri Lanka. Mineralogical Magazine 55, 33–56.

Fernando, G.W.A.R., Hauzenberger, C.A., Baumgartner, L.P., Hofmeister, W., 2003. Modeling of retrograde diffusion zoning in garnet. Evidence for slow cooling of granulites from the Highland Complex of Sri Lanka. Mineralogy and Petrology 78, 53–71.

Fletcher, R.C., 1977. Quantitative theory for metamorphic differentiation in development of crenulation cleavage. Geology 5, 185–187.

Fockenberg, T., 1998. An experimental study of the pressure-temperature stability of MgMgAl pumpellyite in the system MgO-Al_2O_3-SiO_2-H_2O. American Mineralogist 83, 220–222.

Grant, J.A., Weiblen, P.W., 1971. Retrograde zoning in garnet near the second sillimanite Isograd. American Journal of Science 270, 281–296.

Granath, J.W., 1980. Strain, metamorphism, and the development of differentiated crenulation cleavages at Cooma, Australia. The Journal of Geology 88, 589–601.

Hacker, B.R., Goodge, J.W., 1990. Comparison of early Mesozoic high-pressure rocks in the Klamath Mountains and Sierra Nevada. Geological Society of America 277–295. Special Paper 225.

Harley, S.L., 2004. Extending our understanding of ultrahigh temperature crustal metamorphism. Journal of Mineralogical and Petrological Sciences 99, 140–158.

Harley, S.L., 2008. Refining the P-T records of UHT crustal metamorphism. Journal of Metamorphic Geology 26, 125–154.

He, X.F., Santosh, M., Tsunogae, T., Malaviarachchi, S.P.K., 2016a. Early to late neoproterozoic magmatism and magma mixing -mingling in Sri Lanka: implications for convergent margin processes during Gondwana assembly. Gondwana Research 32, 151–180.

He, X.F., Santosh, M., Tsunogae, T., Malaviarachchi, S.P.K., Dharmapriya, P.L., 2016b. Neoproterozoic arc accretion along the 'eastern suture' in Sri Lanka during Gondwana assembly. Precambrian Research 279, 57–80.

Hiroi, Y., Ogo, Y., Namba, K., 1994. Evidence for prograde metamorphic evolution of Sri Lankan pelitic granulites, and implications for the development of continental crust. In: Raith, M., Hoernes, S. (Eds.), Tectonic, Metamorphic and Isotopic Evolution of Deep Crustal Rocks, With Special Emphasis on Sri Lanka. Precambrian Research vol. 66, pp. 245–263.

Hölzl, S., Kröner, H., Kröner, A., Jaeckel, P., Liew, T.C., 1991. Geochronology of the Sri Lankan basement. In: Kröner, A. (Ed.), The Crystalline Crust of Sri Lanka, Part I. Summary of Research of the German- Sri Lankan Consortium. Geological Survey. Department Sri Lanka, Professional. Paper 5, pp. 6–257.

Hölzl, S., Hofmann, A.W., Todt, W., Krönler, H., 1994. U-Pb geochronology of the Sri Lanka basement. In: Raith, M. (Ed.). In: Hoernes, S. (Ed.), Tectonic, Metamorphic and Isotopic Evolution of Deep Crustal Rocks, With Special Emphasis on Sri Lanka. Precambrian Research vol. 66, pp. 123–149.

Jiao, S., Guo, J., Harley, S.L., Windley, B.F., 2013. New constraints from garnetite on the P-T path of the khondalite belt: implications for the tectonic evolution of the North China Craton. Journal of Petroleum 54, 1725–1758.

Kehelpannala, K.V.W., 1991. Structural evolution of high-grade terrains in Sri Lanka with special reference to the areas around Dudangaslanda and Kandy. In: Kroner, A. (Ed.), The Crystalline Crust of Sri Lanka, Part I, Summary of Research of the German- Sri Lankan Consortium. Geological Survey Department, Sri Lanka, Prof. Paper 5, pp. 69–88.

Kehelpannala, K.V.W., 1997. Deformation of a high-grade gondwana fragment, Sri Lanka. Gondwana Research 1, 47–68.

Kehelpannala, K.V.W., 2003. Structural evolution of the middle to lower crust in Sri Lanka—a review. Journal of Geological Society of Sri Lanka 11, 45–86.

Kehelpannala, K.V.W., 2004. Arc accretion around Sri Lanka during the assembly of Gondwana. Gondwana Research 7, 1323–1328.

Kelsey, D.E., Clark, C., Hand, M., Collins, A.S., 2006. Comment on "First report of garnet–corundum rocks from southern India: implications for prograde high-pressure (eclogite-facies?) metamorphism". Earth and Planetary Science Letters 249, 529–534.

Kelsey, D.E., Hand, M., 2015. On ultrahigh temperature crustal metamorphism: phase equilibria, trace element thermometry, bulk composition, heat sources, timescales and tectonic settings. Geoscience Frontiers 6, 311–356.

Kim, H.S., Bell, T.H., 2005. Combining compositional zoning and foliation intersection axes (FIAs) in garnet to quantitatively determine early *P-T-t* paths in multiply deformed and metamorphosed schists: north central Massachusetts, USA. Contributions to Mineralogy and Petrology 149, 141–163.

Kleinschrodt, R., 1994. Large scale thrusting in the lower crustal basement of Sri Lanka. In: Raith, M. (Ed.). In: Hoernes, S. (Ed.), Tectonic, Metamorphic and

Isotopic Evolution of Deep Crustal Rocks, With Special Emphasis on Sri Lanka. Precambrian Research vol. 66, pp. 39–57.
Kretz, R., 1983. Symbols for rock forming minerals. American Mineralogist 68, 277–279.
Kriegsman, L.M., 1989. Deformation and metamorphism in the Trois Seigneurs Massif, Pyrenees-evidence against a rift setting for its Variscan evolution. Netherlands Journal of Geosciences 68, 335–344.
Kriegsman, L.M., 1991. Structural geology of the Sri Lankan basement – a preliminary review. In: Kröner, A. (Ed.), The Crystalline Crust of Sri Lanka, Part I. Summary of Research of the German- Sri Lankan Consortium. Geological Survey. Department Sri Lanka, Professional Paper 5, pp. 52–68.
Kriegsman, L.M., 1993. Structural and petrological investigations into the Sri Lankan high-grade terrain-geodynamic evolution and setting of a Gondwana fragment. Geololgy Ultraiectina 114, 208.
Kriegsman, L.M., 1994. Evidence for a fold nappe in the high-grade basement of central Sri Lanka: terrane assembly in the Pan-African lower crust? Precambrian Research 66, 59–76.
Kriegsman, L.M., 1996. Divariant and trivariant reaction line slopes in FMAS and CFMAS: theory and applications. Contributions to Mineralogy and Petrology 126, 38–50.
Kriegsman, L.M., Schumacher, J.C., 1999. Petrology of sapphirine bearing and associated granulites from central Sri Lanka. Journal of Petrology 40, 1211–1239.
Kröner, A., Cooray, P.G., Vitanage, P.W., 1991. Lithotectonic subdivision of the Precambrian basement in Sri Lanka. In: Kröner, A. (Ed.), The Crystalline Crust of Sri Lanka, Part I. Summary of Research of the German- Sri Lankan Consortium. Geological Survey. Department Sri Lanka, Professional Paper 5, pp. 5–21.
Kröner, A., Jaeckel, P., Williams, I.S., 1994a. Pb-loss patterns in zircons from a high-grade metamorphic terrain as revealed by different dating methods: U-Pb and Pb-Pb ages for igneous and metamorphic zircons from northern Sri Lanka. In: Raith, M., Hoernes, S. (Eds.), Tectonic, Metamorphic and Isotopic Evolution of Deep Crustal Rocks, With Special Emphasis on Sri Lanka. Precambrian Research vol. 66, pp. 151–181.
Kröner, A., Kehelpannala, K.V.W., Kriegsman, L.M., 1994b. Origin of compositional layering and mechanism of crustal thickening in the high-grade gneiss terrain of Sri Lanka. In: Raith, M., Hoernes, S. (Eds.), Tectonic, Metamorphic and Isotopic Evolution of Deep Crustal Rocks, With Special Emphasis on Sri Lanka. Precambrian Research vol. 66, pp. 21–37.
Kröner, A., Kehelpannala, K.V.W., Hegner, E., 2003. Ca. 700–1000 Ma magmatic events and Grenvillian-age deformation in Sri Lanka: relevance for Rodinia supercontinent formation and dispersal, and Gondwana amalgamation. Journal of Asian Earth Sciences 22, 279–300.
Kröner, A., Rojas-Agramonte, Y., Kehelpannala, K.V.W., Zack, T., Hegner, E., Geng, H.Y., Wong, J., Barth, M., 2013. Age, Nd–Hf isotopes, and geochemistry of the Vijayan Complex of eastern and southern Sri Lanka: a Grenville-age magmatic arc of unknown derivation. Precambrian Research 234, 288–321.
Leite, C.M.M., Barbosa, J.S.F., Goncalves, P., Nicollet, C., Sabaté, P., 2009. Petrological evolution of silica-undersaturated sapphirine-bearing granulite in the Paleoproterozoic Salvador–Curaçá Belt, Bahia, Brazil. Gondwana Research 15, 49–70.
Malaviarachchi, S.P.K., Takasu, A., 2011a. Petrology of metamorphic rocks from the Highland and Kadugannawa Complexes, Sri Lanka. Journal of Geology Society of Sri Lanka 14, 103–122.
Malaviarachchi, S.P.K., Takasu, A., 2011b. Electron microprobe dating of monazites from Sri Lanka. Journal of Geology Society of Sri Lanka 14, 81–90.
Malaviarachchi, S.P.K., Dharmapriya, P.L., 2015. Revisiting ultrahigh temperature granulites of Sri Lanka: new prograde and retrograde mineral textures from the Highland Complex. Journal of Indian Institute of Science 95, 159–171.
Mathavan, V.W.K.B.N., Prame, W.K.B.N., Cooray, P.G., 1999. Geology of the high grade Proterozoic terrains of Sri Lanka and the assembly of Gondwana: an update on recent developments. Gondwana Research 2, 237–250.
Mathavan, V., Fernando, G.W.A.R., 2001. Reactions and textures in grossular-wollastonite-scapolite calc-silicate granulites from Maligawila, Sri Lanka. Lithos 59, 217–232.
Milisenda, C.C., Liew, T.C., Hofmann, A.W., Kröner, A., 1988. Isotopic mapping of age provinces in Precambrian high grade terrains: Sri Lanka. Journal of Geology 96, 608–615.
Milisenda, C.C., Liew, T.C., Hofmann, A.W., Köhler, H., 1994. Nd isotopic mapping of the Sri Lanka basement: update, and additional constraints from Sr isotopes. In: Raith, M., Hoernes, S. (Eds.), Tectonic, Metamorphic and Isotopic Evolution of Deep Crustal Rocks, With Special Emphasis on Sri Lanka. Precambrian Research vol. 66, pp. 95–110.
Nasipuri, P., Bhattacharya, A., Das, S., 2009. Metamorphic reactions in dry and aluminous granulites: a Perple_X P–T pseudosection analysis of the influence of effective reaction volume. Contributions to Mineralogy and Petrology 157, 301–311.
Osanai, Y., 1989. A Preliminary Report on Sapphirine/Kornerupine Granulite from Highland Series, Sri Lanka (Extended Abstract). Seminar on recent advantages in Precambrian Geology of Sri Lanka, IFS Kandy, Sri Lanka.
Osanai, Y., Ando, K.T., Miyashita, Y., Kusachi, I., Yamasaki, T., Doyama, D., Prame, W.K.B.N., Jayatilake, S., Mathavan, V., 2000. Geological field work in the southwestern and central parts of the Highland Complex, Sri Lanka during 1998–1999, special reference to the highest grade metamorphic rocks. Journal of Geoscience 43, 227–247.
Osanai, Y., Sajeev, K., Owada, M., Kehelpannala, K.V.W., Prame, W.K.B., Nakano, N., Jayatileke, S., 2006. Metamorphic evolution of ultrahigh-temperature and high-pressure granulites from Highland Complex, Sri Lanka. Journal of Asian Earth Sciences 28, 20–37.
Osanai, Y., Sajeev, K., Nakano, N., Kitano, I., Kehelpannala, K.V.W., Kato, R., Adachi, T., Malaviarachchi, S.P.K., 2016a. UHT granulites of the Highland Complex, Sri Lanka II: geochronological constraints and implications for Gondwana correlation. Journal of Mineralogical and Petrological Sciences 111, 157–169.
Osanai, Y., Sajeev, K., Nakano, N., Kitano, I., Kehelpannala, K.V.W., Kato, R., Adachi, T., Malaviarachchi, S.P.K., 2016b. UHT granulites of the Highland Complex, Sri Lanka I: geological and petrological background. Journal of Mineralogical and Petrological Sciences 111, 145–156.
Passchier, C.W., Trouw, R.A.J., 1996. Microtectonics. Springer-Verlag, Berlin. ISBN 3540587136. 289 pp.
Perera, L.R.K., 1994. P-T-t path vs. isotopic ages in correlations, anti-correlations and pseudocorrelations of regional metamorphic terrains, a case study from Sri Lanka. Journal of Geological Society of Sri Lanka 5, 27–41.
Powell, C.McA., Vernon, R.H., 1979. Growth and rotation history of garnet porphyroblasts with inclusion spirals in a Karakoram schist. Tectonophysics 54, 25–43.
Prakash, D., Sharma, I.N., 2008. Reaction textures and metamorphic evolution of quartz-free granulites from Namlekonda (Karimnagar), Andhra Pradesh, India. International Geology Review 50, 1008–1021.
Prakash, D., Sharma, I.N., 2011. Metamorphic evolution of Karimnagar granulite terrane, Eastern Dharwar Craton, South India. Geological Magazine 48, 112–132.
Prakash, D., Singh, P.Chandra, 2014. New finding of Sillmanite in sapphirine-bearing granulites from Pedapalli, NE part of the Eastern Dharwar Craton, India. Journal of Geological Society of India 84, 29–34.
Prakash, D., Chandra Singh, P., Hokada, T., 2013. A new occurrence of sapphirine-spinel-corundum-bearing granulite from NE of Jagtiyal, Eastern Dharwar Craton, Andhra Pradesh. Journal of Geological Society of India 82, 5–8.
Raase, P., Schenk, V., 1994. Petrology of granulite facies metapelites of the Highland Complex, Sri Lanka: implication for the metamorphic zonation and the *P-T* path. In: Raith, M., Hoernes, S. (Eds.), Tectonic, Metamorphic and Isotopic Evolution of Deep Crustal Rocks, With Special Emphasis on Sri Lanka. Precambrian Research vol. 66, pp. 265–294.
Sajeev, K., Osanai, Y., 2004a. Ultrahigh-temperature metamorphism (1150°C, 12 kbar) and multi-stage evolution of Mg, Al rich granulites from the central Highland Complex, Sri Lanka. Journal of Petrology 45, 1821–1844.
Sajeev, K., Osanai, Y., 2004b. Osumilite and spinel+quartz from Sri Lanka: implications for UHT conditions and retrograde *P–T* path. Journal of Mineralogical and Petrological Sciences 99, 320–327.
Sajeev, K., Osanai, Y., Connolly, J.A.D., Suzuki, S., Ishioka, J., Kagami, H., Rino, S., 2007. Extreme crustal metamorphism during a Neoproterozoic event in Sri Lanka, a study of dry mafic granulites. Journal of Geology 115, 563–582.
Sajeev, K., Williams, I.S., Osanai, Y., 2010. Sensitive high-resolution ion microprobe U-Pb dating of prograde and retrograde ultrahigh-temperature metamorphism as exemplified by Sri Lankan granulites. Geology 38, 971–974.
Santosh, M., Tsunogae, T., Malaviarachchi, Sanjeewa P.K., Zhang, Z.M., Ding, H.X., Tang, L., Dharmapriya, P.L., 2014. Neoproterozoic crustal evolution in Sri Lanka: insights from petrologic, geochemical and zircon U–Pb and Lu–Hf isotopic data and implications for Gondwana assembly. Precambrian Research 255, 1–29.
Sato, K., Santosh, M., Tsunogae, T., 2010. High *P-T* phase relation of magnesian (Mg0.7Fe0.3) staurolite in the system FeO-MgO-Al_2O_3-SiO_2-H_2O: implications for prograde high-pressure history of ultrahigh-temperature metamorphic rocks. American Mineralogist 95, 177–184.
Sawyer, E.W., 2001. Melt segregation in the continental crust: distribution and movement of melt in anatectic rocks. Journal of Metamorphic Geology 19, 291–309.
Schreyer, W., 1988. Experimental studies of metamorphism of crustal rocks under mantle pressures. Mineralogical Magazine 52, 1–26.
Schumacher, R., Faulhaber, S., 1994. Summary and discussion of P-T estimates from garnet-pyroxene-plagioclase-quartz bearing granulite facies rocks from Sri Lanka. In: Raith, M., Hoernes, S. (Eds.), Tectonic, Metamorphic and Isotopic Evolution of Deep Crustal Rocks, With Special Emphasis on Sri Lanka. Precambrian Research vol. 66, pp. 295–308.
Schoneveld, C., 1977. A study of some typical inclusion patterns in strongly paracrystalline-rotated garnets. Tectonophysics 39, 453–471.
Sharib, A.S.A.A.A., Bell, T.H., 2011. Radical changes in bulk shortening directions during orogenesis: Significance for progressive development of regional folds and thrusts. Precambrian Research 188, 1–20.
Sharma, I.N., Prakash, D., 2008. A new occurrence of sapphirine-bearing granulite from Podur, Andhra Pradesh. Mineralogy and Petrology 92, 415–425.
Spear, F.S., Cheney, J.T., 1989. A petrogenetic grid for pelitic schists in the system SiOr-Al_2O_3-FeO-MgO-K_2O-H_2O. Contributions to Mineralogy and Petrology 101, 149–164.
Stüwe, K., 1997. Effective bulk composition changes due to cooling: a model predicting complexities in retrograde reaction textures. Contributions to Mineralogy and Petrology 129, 43–52.
Takamura, Y., Tsunogae, T., Santosh, M., Malaviarachchi, S.P.K., Tsutsumi, Y., 2016. U-Pb geochronology of detrital zircon in metasediments from Sri Lanka: implications for the regional correlation of Gondwana fragments. Precambrian Research 281, 434–452.
Touret, J., 1965. Structure of veined gneisses of the Vegârshei massif (Norway Southern). Geological Society of France 3, 104 (in French language).
Tracy, R.J., Robinson, P., Thompson, A.B., 1976. Garnet composition and zoning in the determination of temperature and pressure of metamorphism, central Massachusetts. American Mineralogist 61, 762–775.

Tsunogae, T., van Reenen, D.D., 2006. Corundum + quartz and Mg-staurolite bearing granulite from the Limpopo Belt, southern Africa: implications for a *P-T* path. Lithos 92, 576–587.

Tsunogae, T., van Reenen, D.D., 2011. High-pressure and ultrahigh-temperature granulite-facies metamorphism of Precambrian high-grade terranes: case study of the Limpopo Complex. In: van Reenen, D.D., Kramers, J.D., McCourt, S., Perchuk, L.L. (Eds.), Origin and Evolution of Precambrian High-Grade Gneiss Terranes, With Special Emphasis on the Limpopo Complex of Southern Africa. Geological Society of America Memoir, vol. 207, pp. 107–124.

Tuccillo, M.E., Essene, E.J., Van der Pluijm, B.A., 1990. Growth and retrograde zoning in garnets from highgrade metapelites: implications for pressure-temperature paths. Geology 18, 839–842.

Vielzeuf, D., Holloway, J.R., 1988. Experimental determination of the fluid-absent melting relations in the pelitic system. Consequences for crustal differentiation. Contributions to Mineralogy and Petrology 98, 257–276.

Voll, G., Kleinschrodt, R., 1991. Sri Lanka: structural, magmatic and and metamorphic development of a Gondwana fragment. In: Kröner, A. (Ed.), The Crystalline Crust of Sri Lanka, Part I. Summary of Research of the German-Sri Lankan Consortium. Geological Survey Department, Sri Lanka, Professional Paper 5, pp. 22–52.

White, R.W., Powell, R., Clarke, G.L., 2003. Prograde metamorphic assemblage evolution during partial melting of metasedimentary rocks at low pressures: migmatites from Mt Stafford, Central Australia. Journal of Petrology 44, 1–4.

Williams, P.F., 1972. Development of metamorphic layering and cleavage in low-grade metamorphic rocks at Bermagui, Australia. American Journal of Science 272, 1–47.

Williams, M.L., Scheltema, K.E., Jercinovic, M.J., 2001. High-resolution compositional mapping of matrix phases: implications for mass transfer during crenulation cleavage development in the Moretown Formation, western Massachusetts. Journal of Structural Geology 23, 923–939.

Yardley, B.W.D., 1977. An empirical study of diffusion in garnet. American Mineralogist 62, 793–800.

Yoshida, M., Kehelpannala, K.V.W., Hiroi, Y., Vitanage, P.W., 1990. Sequence of deformation and metamorphism of granulites of Sri Lanka. Journal of Geosciences, Osaka City University 33, 69–107.